Forum for Electromagnetic Research Methods and Application Technologies (FERMAT)

Effects of Antenna Radiation on Coherent Back-Scattering from the Ocean Surface

Jimmy O. Alatishe (1) and Wasyl Wasylkiwskyj (2)
(1) The U.S. Naval Research Laboratory, Washington DC 20375
(Email: jimmy.alatishe@nrl.navy.mil)
(2) The George Washington University, Washington DC 20052
(Email: wasylkiw@gwu.edu)

Abstract—**The analytical model previously developed by the authors for backscattering from a random air-dielectric interface is used to investigate the effects of coherence in the backscattered field on the monostatic radar cross-section (RCS) of the sea. The sea-surface is represented by several empirical wave-number spectra for a fully developed sea, namely, the Pierson-Neumann Spectrum, Pierson-Moskowitz Spectrum, and the Elfouhaily Unified Spectrum. A Generalized Normalized Radar Cross-Section (GNRCS) is introduced as a metric of the combined effects of coherence and antenna radiation characteristics. By employing a small-slope approximation (SSA) of the sea surface, the relative powers of the signal returns are computed and compared to the signal-power returns based on data-derived normalized RCS X-band (NRCS) (σ^0) values for the corresponding simulated sea state. The objective of this analysis is to assess the effects of spatial coherence on backscattering using a GNRCS through validation with σ^0 obtained from measurements of sea backscatter.**

Index Terms— **Generalized Normalized Radar Cross Section (GNRCS), Antenna Reciprocity, Ocean Backscattering, Antenna Radiation Pattern.**

I. INTRODUCTION

Normally, the assessment of radar-clutter returns from a distributed target (that is land, sea, etc.) is based on models that discretize the scattering contributions from within the antenna footprint [1]. The surface within the main beam footprint is treated as a random distribution of point scatterers with no mutual interaction. The individual contributions from the point scatterers are taken as proportional to the respective incident signal powers and summed. To maintain consistency, the vertical displacement of the surface is modeled as a random process, with no consideration for the spatial correlation within the beam footprint. Based on these assumptions, the relative power of the radar clutter is estimated by evaluating the surface integral of the gain-squared divided by the fourth power of the range to the local region encompassed by the antenna footprint, and multiplying the result by the normalized radar cross-section (NRCS) [1], or σ^0 as it is commonly known. Thus, stated explicitly,

$$\frac{P_{rec}}{P_{trans}} = \frac{\lambda^2}{(4\pi)^3}\int \frac{G^2(\theta,\phi)}{R^4}\sigma^0 dS.$$

The NCRS is the most important metric in the characterization of radar clutter and its properties are assumed to be independent of the antenna radiated-field features within the illuminated region of the surface. For the most part, σ^0 is considered to be separable from the variables entering into the surface integral and is determined by its direct inversion.

Obtaining σ^0 with this technique requires that the illumination within the area contributing to backscattering be constant. However, when the clutter originates from a non-uniformly illuminated patch of the sea surface (say the entire antenna footprint) the validity of this inversion technique is questionable since it entirely ignores any spatial correlation among the clutter returns from different regions of the antenna footprint. In addition, the assumption associated with the inversion technique fails to take into account of the statistical and physical properties of the surface as well as of the antenna radiation pattern. This is represented in a number of examples in the literature. For instance, in [2], [3], [4], and [5] the gain and polarization were assumed to be uniform throughout the antenna footprint. Here the gain and polarization contributions from the center of the main lobe of the antenna pattern are taken to be the only values of interest. In [6], [7], and as discussed in [8], the uncorrelated scattered field assumption is enforced based on the decorrelation times of the radar returns.

It has been demonstrated that the measured radar cross-section (RCS) per unit area of a rough surface depends on both the kinematic and stochastic properties of the rough

This use of this work is restricted solely for academic purposes. The author of this work owns the copyright and no reproduction in any form is permitted without written permission by the author.

surface as well as on the properties of the receiving (transmitting) antenna radiation and polarization patterns [9]. In addition, formulations of σ^0, which incorporate the effects of spatial coherence, have been investigated in [10] and [11]. A most important feature is illustrated in [10], where the author distinguishes the difference between the NRCS generated by a plane wave and an antenna illuminating a rough surface. Herein, the author establishes a criterion for the NRCS being equal for both types of illumination; provided that the radii of curvature of surface are small compared to the antenna footprint. However, these attempts assume an incoherent scattering model and/or only consider the radar returns from the beam center of the antenna pattern. An approach to modeling backscattering from randomly perturbed surfaces is presented in [8] and is capable of incorporating these effects. That model was subsequently applied in [12] in a study of spatial-coherence effects of the electromagnetic field backscattered by an irregular dielectric-air interface. In this paper, an extension of the formulation of [12] is applied to the analysis of radar ocean clutter using a modified version of the small-slope approximation (SSA). The wave-number spectra of the ocean surface are represented by the Pierson-Moskowitz, the Pierson-Neumann, and the Elfouhaily unified wave-number spectra for a fully developed sea. As a measure of back-scattered power, σ^0 is replaced by the Generalized NCRS (GNRCS) per unit area which incorporates the effects of correlation of the backscattered field as well as its dependence on the relevant antenna parameters as observed within the footprint. Stated explicitly, embedded in the formulation of the GNRCS are:

- the statistical and physical properties of the surface;
- the kinematic description of the surface;
- the gain and polarization generated by the antenna.

Numerical results are presented in terms of the average relative received power as a function of wind speed, wind direction, antenna radiation pattern, and polarization, and compared with the corresponding relative received powers based on measured σ^0 at X-Band. Lastly, we establish the product of the antenna gain and GNRCS as a metric for the combined effects of spatial coherence of the surface and antenna radiation characteristics within the footprint. The objective is to assess the effects of spatial coherence on backscattering using the GNRCS through validation with σ^0 obtained from measurements of sea backscatter.

II. RCS BASED ON AN INCOHERENT SCATTERING MODEL

An antenna at mean height H above the ocean surface is shown in Fig. 1. The Cartesian coordinate system serving as a reference for the spherical coordinates θ and ϕ is indicated by the red axes. The antenna can be beam steered in elevation to $\theta = \overline{\theta}$, and in azimuth $\phi = \overline{\phi}$ .The antenna gain will have its maximum at $\theta = \overline{\theta}$, $\phi = \overline{\phi}$ corresponding to the position vector $\overline{\mathbf{R}}$. The position vector $\mathbf{R}$ is directed from the phase center of the antenna to a given point on the rough surface with magnitude $R = \sqrt{x^2 + y^2 + (H - \varsigma(x,y))^2}$. For $\varsigma(x,y) = 0$, $R \equiv R_s = \sqrt{x^2 + y^2 + H^2}$.

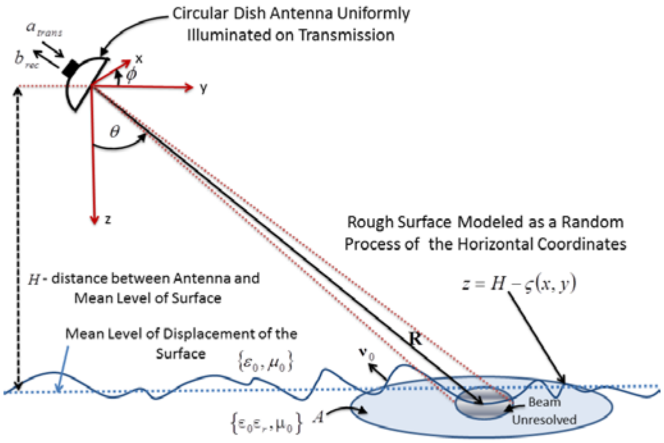

Circular Dish Antenna Uniformly Illuminated on Transmission
a_{trans}
b_{rec}
x
ϕ
y
θ
z
Rough Surface Modeled as a Random Process of the Horizontal Coordinates
H - distance between Antenna and Mean Level of Surface
$z = H - \varsigma(x, y)$
Mean Level of Displacement of the Surface
$\{\varepsilon_0, \mu_0\}$
R
$\mathbf{v}_0$
Beam Unresolved
$\{\varepsilon_0\varepsilon_r, \mu_0\}$
A

Fig. 1. Scattering geometry and antenna footprint

The solid angle $\Omega_{Antenna}$ determines the area of the beam footprint A on the surface. A beam-unresolved scatterer is defined as a scatterer that subtends a solid angle $\Omega_{scatterer}$ much smaller than $\Omega_{Antenna}$. As a result, the field incident on the scatterer can be approximated by a plane wave and the receiver-to-transmitter transfer function can be expressed by [8] :

$$\frac{b_{rec}}{a^*_{trans}} = \frac{-2\pi j}{k_0} \frac{G(\theta,\phi)}{4\pi R^2} \left(\sqrt{\frac{\sigma}{4\pi}} \right) \mathbf{p}_t \cdot \mathbf{p}_s e^{-2jk_0 R}, \tag{1}$$

where a_{trans} is the stimulus from the transmitter, b_{rec} is the response due to the impinging plane wave, the scattering cross section of a scatterer σ is approximated by the small patch of the illuminated surface and $G(\theta,\phi)$ is the available antenna gain. The $\mathbf{p}_t$ and $\mathbf{p}_s$ are the (complex) polarization vectors, respectively, of the transmitted and scattered fields, all evaluated at (θ,ϕ). When $\Omega_{Antenna} \ll \Omega_{scatterer}$, we speak of a beam-resolved scatterer for which the calculation of the receiver response requires an integration of (1) over $\Omega_{Antenna}$. Radar clutter estimates are generally based on an incoherent integration (summation). This amounts to summing the squared magnitude of (1) weighted with the differential cross section $d\left(\sigma \left|\mathbf{p}_t \cdot \mathbf{p}_s\right|^2\right) \equiv \sigma^0 dS$, where dS is the differential area. As a result one obtains

$$\left\langle \left| \frac{b_{rec}}{a_{trans}} \right|^2 \right\rangle = \frac{\lambda^2}{(4\pi)^3} \int \frac{G^2(\theta,\phi)}{R^4} \sigma^0 dS, \tag{2}$$

which is just the average of the ratio of received-to-transmitter available power.

The usual approach in finding σ^0 from (2) is to assume that within the main beam (for all practical purposes at the beam peak) σ^0 is constant and simply invert (2). One problem with this procedure is that it fails to take account of contributions originating outside the main beam however defined. Within the main beam, no account is taken of incoherent addition as a potential source of errors. It appears that the justification for incoherent processing rests mainly on its relative simplicity. Another common idealization is to entirely ignore the intrinsic dependence of σ^0 on the antenna radiation field. This dependence has been identified in [8], [10], and [12], and is incorporated into the GNRCS discussed in the sequel.

.

III. COHERENT SCATTERING AND THE GNRCS

As given in [8] and elaborated on in [12], the receive-transmit transfer function linking the transmitter output a_{trans} with the response to the backscattered field b_{rec} can be put into the form:

$$\frac{b_{rec}}{a_{trans}} = \frac{-2\pi j a^{*}_{trans}}{k_0 a_{trans}} \int\!\!\int_A \frac{G(\theta,\phi)}{4\pi R^2} \mathbf{p_r} \cdot \mathbf{S}_{distr}(\theta,\phi) \cdot \mathbf{p_r} e^{-j2k_0 R} d^2\mathbf{R}, \tag{3}$$

where $\mathbf{S}_{distr}(\theta,\phi)$ is a 2×2 scattering matrix determined by the back-scattering characteristics of a rough air/dielectric interface. The scattering parameters (in the network sense) a_{trans} and b_{rec} are normalized such that $|b_{rec}|^2$ and $|a_{trans}|^2$ represent, respectively, the received power and the transmitter available power. The transmitter polarization vector $\mathbf{p_r}$ is defined by

$$\mathbf{p_r} = \frac{\mathbf{F}_{rad}(\theta,\phi)}{|\mathbf{F}_{rad}(\theta,\phi)|} \tag{4}$$

and $|\mathbf{F}_{rad}(\theta,\phi)|^2$ represents radiated power per steradian. Accordingly, the available antenna gain is

$$G(\theta,\phi) = 4\pi \left| \frac{\mathbf{F}_{rad}(\theta,\phi)}{a_{trans}} \right|^2 .$$

Note that the expression in (3) is the antenna reciprocity relationship for a given antenna irradiated by an arbitrary electromagnetic field. Equation (3) was derived from the now classical treatment which utilizes network parameters to give a full description of the electromagnetic phenomena of any antenna. This includes parameters like gain, polarization, aspect ratio, radiation efficiency, scattering, etc. Further details regarding the derivation of (3) are addressed in [13], [14], and [15].

Based on (3), the average of the ratio of received-to-transmitter available power is

$$\left\langle \left| \frac{b_{rec}}{a_{trans}} \right|^2 \right\rangle = \lambda^2 \left\langle \left| \int\!\!\int_A \frac{G(\theta,\phi)}{4\pi R^2} \mathbf{p_r} \cdot \mathbf{S}_{distr}(\theta,\phi) \cdot \mathbf{p_r} e^{-j2k_0 R} d^2\mathbf{R} \right|^2 \right\rangle . \tag{5}$$

To assess the consequences of approximating coherent scattering by incoherent scattering, we transform (5) into a form resembling (2). To this end, we first represent the differential $d^2\mathbf{R}$ in terms of its projection on the xy plane

$$d^2\mathbf{R} = s(\theta,\phi)\,dxdy = s(\theta,\phi)\,dS \equiv \sqrt{1 + |\nabla_t \varsigma(x,y)|^2}\,dS$$

and define a new scattering variable

$$Q(\theta,\phi) = s(\theta,\phi)\mathbf{p_r} \cdot \mathbf{S}_{distr}(\theta,\phi) \cdot \mathbf{p_r} e^{-j2k_0 R(\theta,\phi)} .$$

Factoring (5) and averaging only the product of the scattering variables yields

$$\left\langle \left| \frac{b_{rec}}{a_{trans}} \right|^2 \right\rangle = \lambda^2 \int\!\!\int_A \frac{G(\theta,\phi)}{4\pi R^2} \int\!\!\int_A \frac{G(\theta',\phi')}{4\pi R'^2} \langle Q(\theta,\phi) Q(\theta',\phi') \rangle dS' dS .$$

After rearranging the terms in the first integrand, we get

$$\left\langle \left| \frac{b_{rec}}{a_{trans}} \right|^2 \right\rangle = \frac{\lambda^2}{(4\pi)^3} \int\!\!\int_A \frac{G^2(\theta,\phi)}{R^4} dS \frac{4\pi R^2}{G(\theta,\phi)} \int\!\!\int_A \frac{G(\theta',\phi')}{R'^2} \langle Q(\theta,\phi) Q(\theta',\phi') \rangle dS'$$
$$= \frac{\lambda^2}{(4\pi)^3} \int\!\!\int_A \frac{G^2(\theta,\phi)}{R^4} \sigma(S)\,dS .$$

The last equation has the form of (2) with σ^0 replaced by

$$\sigma(S) = \frac{4\pi R^2}{G(\theta,\phi)} \int\!\!\int_A \frac{G(\theta',\phi')}{R'^2} \langle Q(\theta,\phi) Q(\theta',\phi') \rangle dS', \tag{6}$$

which we define as the GNRCS. The GNRCS is not only a function of the radiation field (including its polarization) of the antenna, but also of the kinematics and statistics of the surface. As can be seen from (6), in regions where $G(\theta,\phi)$ is constant it can be removed from the integrand and cancelled with the gain function in the denominator. In that case, the GNRCS becomes independent of the antenna gain. However, this cancellation applies only to the gain and not to the polarization. Thus, in general, the GNRCS is polarization dependent. In view of (5), this dependence enters as an interaction between the antenna polarization and the scattering characteristics of the surface.

Note that (6) reduces to $\sigma^0(\theta,\phi)$ when

$$\left\langle Q(\theta,\phi)Q(\theta',\phi')\right\rangle \sim \gamma\left|\hat{f}(\theta,\phi)\right|^2 \delta\left(\boldsymbol{\rho}-\boldsymbol{\rho}'\right),$$

which corresponds to incoherent scattering. That is, if all of the surface properties are known to be statistically uncorrelated, then

$$\sigma(S)=\sigma(\theta,\phi)\rightarrow\sigma^0(\theta,\phi)=4\pi\gamma\left|\hat{f}(\theta,\phi)\right|^2. \tag{7}$$

The parameter γ is some measure of the root-mean squared (RMS) height, slope, and/or horizontal correlation distance of the surface compared to k_0. On physical grounds $\hat{f}(\theta,\phi)$ must encompass the polarization of the equivalent fields and constitutive properties of the surface in A. From an empirical standpoint, the σ^0 obtained from the ocean (or from any rough surface) is just the average or mean value of $\sigma(S)$ given by

$$\sigma^0=\frac{\iint\limits_A \sigma(S)\,dS}{A};\ A=\iint\limits_A dS. \tag{8}$$

In examining (6) or (7), it is seen that properties of the surfaces are generally not separable for direct inversion for computing σ^0. It is the opinion of the authors that the best way to characterize ocean clutter is through the received power at the port, because that is what is actually measured, and not σ^0.

IV. SSA OF THE SCATTERING MATRIX AND THE GNRCS

The preceding rather general approach to surface scattering follows closely that presented in [8] (see Appendix A). These results are purely formal for they omit the crux of the problem, which is determining the scattering matrix (see Appendix B). Again, as outlined in [8] in its full generality, we are dealing with a complex boundary-value problem so that analytical results invariably employ some form of approximation. This paper employs the simplification introduced in [12] using an approximation closely linked to what has been referred to as the Rayleigh hypothesis [16]. In our interpretation, it amounts to approximating the fields scattered by an irregular boundary by the Fourier transform of the field scattered by an equivalent planar surface. This approximation is difficult to justify theoretically so that its validation must come indirectly from experimental data. Using this formulation, one can find the scattering matrix using perturbations either for small amplitudes (that is, $|k_0\varsigma \ll 1|$) or for small slopes,

$$\left|\nabla_t\varsigma(x,y)\right|\ll 1;\nabla_t\varsigma(x,y)=\left\{\frac{\partial\varsigma(x,y)}{\partial x},\frac{\partial\varsigma(x,y)}{\partial y}\right\}.$$

Only the SSA, or rather a modified version of it, is used in this paper and follows closely the exposition in [12]. The conventional formulation, using the SSA for scattering by an irregular boundary, is presented in [16]. Unlike in the present paper, the emphasis is on scattering per se with the antenna playing only an indirect role. Under the modified SSA the scattering matrix, restated directly from [12], Eq. 24, is

$$S_{distr}(\theta,\phi)=\frac{k_0\cos\theta}{\pi}\sin\left[k_0\varsigma(\boldsymbol{\rho})\cos\theta\right]\begin{bmatrix}\Gamma'(\theta) & 0\\ 0 & -\Gamma''(\theta)\end{bmatrix}, \tag{9}$$

where $\Gamma'(\theta)$ and $\Gamma''(\theta)$ are the Fresnel reflection coefficients for parallel and perpendicular polarizations, respectively, at the mean level of the surface H in Fig. 1. Note that unless $|k_0\varsigma(x,y)\ll 1|$, the scattering matrix is a nonlinear function of $k_0\varsigma(\boldsymbol{\rho})$. This nonlinear dependence corresponds to large vertical surface displacements (wave heights) compared to the radar wavelength. It is worth noting that $\varsigma(\boldsymbol{\rho})$ is a relative displacement with respect to the mean height H and is not affected by a displacement of the irregular surface in the vertical direction in this treatment.

Small slopes force $s(\theta,\phi)=\sqrt{1+\left|\nabla_t\varsigma(x,y)\right|^2}$ in (6) to unity, and since the antenna is sufficiently far away from the surface $R\sim R_s-\varsigma(\boldsymbol{\rho})\cos\theta$, (6) assumes the form

$$\sigma(S)=\frac{4k_0^2R_s^2e^{-j2k_0R_s}}{\pi G(\theta,\phi)}\cdot \iint\limits_A\frac{G(\theta',\phi')e^{j2k_0R_s'}}{R_s'^2}\left\langle\begin{array}{l}\left(\mathbf{p_r}\cdot\mathbf{S}_{distr}(\theta,\phi)\cdot\mathbf{p_r}e^{j2k_0\varsigma(\boldsymbol{\rho})\cos\theta}\right)\cdot\\ \left(\mathbf{p_r}'^*\cdot\mathbf{S}^*_{distr}(\theta',\phi')\cdot\mathbf{p_r}'^*e^{-j2k_0\varsigma(\boldsymbol{\rho}')\cos\theta'}\right)\end{array}\right\rangle dS'. \tag{10}$$

The terms in the expectation operator in (10) are direct complex-conjugate pairs in which the products can be simplified to

$$\mathbf{p_r}\cdot\mathbf{S}_{distr}(\theta,\phi)\cdot\mathbf{p_r}=\sin\left[k_0\varsigma(\boldsymbol{\rho})\cos\theta\right]f_s(\theta,\phi). \tag{11}$$

where $f_s(\theta,\phi)$ is the polarization factor under the modified SSA, which is equal to

$$f_s(\theta,\phi)=\cos\theta\left[p_\theta^2(\theta,\phi)\Gamma'(\theta)-p_\phi^2(\theta,\phi)\Gamma''(\theta)\right]. \tag{12}$$

The product of $\sin\left[k_0\varsigma(\boldsymbol{\rho})\cos\theta\right]$ and $e^{j2k_0\varsigma(\boldsymbol{\rho})\cos\theta}$ in the ensemble expectation operator in (10) is also represented by a set of complex conjugate pairs. This product is expressed as

$$\Psi_s(\theta,\phi) = \sin\left[k_0\varsigma(\boldsymbol{\rho})\cos\theta\right]e^{j2k_0\varsigma(\boldsymbol{\rho})\cos\theta} = \frac{\left[e^{j3k_0\varsigma(\boldsymbol{\rho})\cos\theta} - e^{jk_0\varsigma(\boldsymbol{\rho})\cos\theta}\right]}{2j}. \qquad (13)$$

A simplification is achieved when the narrow-beam approximation is applied to (10) with the result

$$R_s \cong \bar{R} + \boldsymbol{\rho}\cdot\bar{\boldsymbol{\rho}}_0\sin\bar{\theta} \qquad (14)$$

The unit vector $\bar{\boldsymbol{\rho}}_0$ is defined as $\bar{\boldsymbol{\rho}}_0 = \bar{\mathbf{x}}_0\cos\bar{\phi} + \bar{\mathbf{y}}_0\sin\bar{\phi}$, where $\bar{\phi}$ is the antenna azimuth-beam steering angle. If the appropriate substitutions are made in (11) using (12), (13), and (14), then the GNRCS under the SSA is expressed as

$$\sigma(S) = \frac{4k_0^2 f_s(\theta,\phi)}{\pi G(\theta,\phi)}\cdot \iint_A G(\theta',\phi')\, f_s^*(\theta',\phi')\, e^{j2k_0\sin\bar{\theta}\left(\boldsymbol{\rho}-\boldsymbol{\rho}'\right)\cdot\bar{\boldsymbol{\rho}}_0}\left\langle \Psi_s(\theta,\phi)\Psi_s^*(\theta',\phi')\right\rangle dS'. \qquad (15)$$

Equation (15) relates the material properties of the surface and the electromagnetic properties of the backscattered field within A, to the spatial coherence of the surface as characterized by the quantities $\left\langle \Psi_s(\theta,\phi)\Psi_s^*(\theta',\phi')\right\rangle$ and $e^{j2k_0\sin\bar{\theta}\left(\boldsymbol{\rho}-\boldsymbol{\rho}'\right)\cdot\bar{\boldsymbol{\rho}}_0}$. The term $\left\langle \Psi_s(\theta,\phi)\Psi_s^*(\theta',\phi')\right\rangle$ is the expected value of the Hermitian product of the phase-factor $\Psi_s(\theta,\phi)$, which is related to the impedance seen at the antenna port due to the vertical displacement $\varsigma(\boldsymbol{\rho})$. The name "phase-factor" was selected because $\varsigma(\boldsymbol{\rho})$ enters into the argument of the complex exponential in (13). An expression for $\left\langle \Psi_s(\theta,\phi)\Psi_s^*(\theta',\phi')\right\rangle$ can, in general, not be given explicitly until the joint probability density function (PDF) of $\varsigma(\boldsymbol{\rho})$ is specified. For the ocean surface, the PDF can be constructed empirically through tedious experimentation. The results of these methods have not yet produced reliable PDFs and are not employed in this investigation.

Continuing onward, $\left\langle \Psi_s(\theta,\phi)\Psi_s^*(\theta',\phi')\right\rangle$ is expressed as the sum of the characteristic functions for the different spatial spectral weights k_{α_n} and k_{β_n}, which are directly derived from the inner and outer algebraic product terms of $\Psi_s(\theta,\phi)\Psi_s^*(\theta',\phi')$ or,

$$\left\langle \Psi_s(\theta,\phi)\Psi_s^*(\theta',\phi')\right\rangle = \frac{1}{4}\sum_{n=1}^{4}(-1)^{n+1}\left\langle e^{jk_{\alpha_n}\varsigma(\boldsymbol{\rho})}e^{-jk_{\beta_n}\varsigma\left(\boldsymbol{\rho}'\right)}\right\rangle,$$
$$\left\{k_{\alpha_1},k_{\alpha_2},k_{\alpha_3},k_{\alpha_4}\right\} = \left\{3k_0\cos\theta, 3k_0\cos\theta, k_0\cos\theta, k_0\cos\theta\right\};$$
$$\left\{k_{\beta_1},k_{\beta_2},k_{\beta_3},k_{\beta_4}\right\} = \left\{3k_0\cos\theta', k_0\cos\theta', k_0\cos\theta', 3k_0\cos\theta'\right\}. \qquad (16)$$

For the purposes of this investigation, the PDF of $\varsigma(\boldsymbol{\rho})$ is chosen to be a Gaussian random process with autocorrelation function $\Re(\boldsymbol{\rho}-\boldsymbol{\rho}')$ and $\psi(\boldsymbol{\kappa})$ wave-number spectrum.

Equation (16) then assumes the form

$$\left\langle \Psi_s(\theta,\phi)\Psi_s^*(\theta',\phi')\right\rangle = \frac{1}{4}\sum_{n=1}^{4}(-1)^{n+1}e^{-\frac{\chi_n}{2}} \qquad (17)$$

with

$$\chi_n = \left\{\begin{bmatrix} k_{\alpha_n} \\ -k_{\beta_n}\end{bmatrix}^T \begin{bmatrix} \sigma_{\varsigma\varsigma}^2 & \Re(\boldsymbol{\rho}-\boldsymbol{\rho}') \\ \Re(\boldsymbol{\rho}-\boldsymbol{\rho}') & \sigma_{\varsigma\varsigma}^2\end{bmatrix}\begin{bmatrix} k_{\alpha_n} \\ -k_{\beta_n}\end{bmatrix}\right\}$$
$$= k_0^2\sigma_{\varsigma\varsigma}^2\left(\alpha_n^2\cos^2\theta + \beta_n^2\cos^2\theta' - 2\alpha_n\beta_n\cos\theta\cos\theta'\,\tfrac{\Re(\boldsymbol{\rho}-\boldsymbol{\rho}')}{\sigma_{\varsigma\varsigma}^2}\right) \qquad (18)$$

where $\left\{\alpha_1,\alpha_2,\alpha_3,\alpha_4\right\} = \left\{3,3,1,1\right\}$ and $\left\{\beta_1,\beta_2,\beta_3,\beta_4\right\} = \left\{3,1,1,3\right\}$, and $\sigma_{\varsigma\varsigma}^2$ is the square of the RMS vertical displacement $\varsigma(\boldsymbol{\rho})$. Substituting (17) and (18) into (15) yields

$$\sigma(S) = \frac{4k_0^2 f_s(\theta,\phi)}{\pi G(\theta,\phi)}\iint_A G(\theta',\phi')\, f_s^*(\theta',\phi')\, e^{-j2k_0\sin\bar{\theta}\left(\boldsymbol{\rho}-\boldsymbol{\rho}'\right)\cdot\bar{\boldsymbol{\rho}}_0}\cdot$$
$$\left\{\frac{1}{4}\sum(-1)^{n+1}\exp\left[\frac{-\varsigma_{0,rms}^2}{2}\begin{pmatrix}\alpha_n^2\cos^2\theta + \beta_n^2\cos^2\theta' \\ -2\alpha_n\beta_n\cos\theta\cos\theta'\,\tfrac{\Re(\boldsymbol{\rho}-\boldsymbol{\rho}')}{\sigma_{\varsigma\varsigma}^2}\end{pmatrix}\right]\right\}dS' \qquad (19)$$

where $\varsigma_{0,rms}^2 = k_0^2\sigma_{\varsigma\varsigma}^2$. Equation (19) represents the GNRCS of a Gaussian random surface illuminated by a narrow-beam antenna. Note that the integrand includes the factor $e^{-j2k_0\sin\bar{\theta}\left(\boldsymbol{\rho}-\boldsymbol{\rho}'\right)\cdot\bar{\boldsymbol{\rho}}_0}$, which, as shown in [12], in the limit of constant gain (and polarization) over the antenna beam footprint, leads to Bragg scattering.

Recall that Eq. (19) is valid only for surfaces that obey the constraint $\left|\nabla_t\varsigma(x,y)\right| \ll 1$ at every point on the surface. Thus, (19) does not apply to spatially uncorrelated surfaces since it diverges when $\Re(\boldsymbol{\rho}-\boldsymbol{\rho}')$ is replaced by $\delta(\boldsymbol{\rho}-\boldsymbol{\rho}')$. To further illustrate this, it is known that for uncorrelated surfaces the mean-square slope $\nabla_t^2\Re(\boldsymbol{\rho})\Big|_{\boldsymbol{\rho}=0}$ cannot be small.

Hence, $\sigma(S)$ cannot be based on an incoherent scattering model. On the other hand, when in addition to small slopes one also assumes small amplitudes, that is with $\left|k_0\varsigma(\boldsymbol{\rho})\right| \ll 1$, the exponential in (19) can be replaced by a linear function of $\Re(\boldsymbol{\rho}-\boldsymbol{\rho}')$ so that (19) becomes compatible with an incoherent scattering model. As shown in equation (36) of [12], this compatibility is a general feature of the small amplitude approximation (SAA), independent of the constraint on the surface slopes. This feature does not imply that the SAA requires incoherence. The choice of the correlation function is arbitrary and can be chosen to model surface scattering where coherence is essential, as, for example in Bragg scattering [12].

V. SIMULATION OF THE GNRCS AND COMPARISONS WITH PUBLISHED DATA

Plots of $\left\langle \left| b_{rec} / a_{trans} \right|^2 \right\rangle$ as a function of the (elevation) beam-steering angle computed using (5) and (6), with $\sigma(S)$ represented by (19), are shown in Figs. 2 and 3. The plots are for the three aforementioned wave-number spectra and are identified in the legend with an "S" for simulated. Also, shown for comparison are plots of $\left\langle \left| b_{rec} / a_{trans} \right|^2 \right\rangle$ (or (2)) derived from published data of σ^0 for 4 m/s wind speed at crosswind. The plots for the horizontal polarization are shown in Fig. 2 and those for the vertical polarization are shown in Fig. 3. Similar results for wind speeds of 5 m/s are shown in Figs. 4 and 5. These simulations were conducted for the given sea-surface conditions at X-Band (10 GHz) and dielectric constant $\varepsilon_r = 55.85 - j37.71$. The antenna is a circular dish, uniformly illuminated on transmission, and with a 16-wavelength diameter (0.48 m) placed 1,000 wavelengths (30 m) above the sea surface (Fresnel number 0.064). The average relative received power at the antenna port was computed for a given beam-steering angle ranging from 0° to 75° in 1° increments in elevation with the azimuth steering angle fixed at 90°. The simulated curves for $\sigma(S)$ in each figure are plotted in solid lines, with magenta for the ocean surface modeled by $\psi(\boldsymbol{\kappa})$ for the Elfouhaily Unified spectrum [17], light green for the Pierson-Neumann spectrum [18], and blue for the Pierson Moskowitz spectrum [19]. Details of the corresponding wave-number spectra can be found in [18], [19], and [17]. The data representing the median RCS per unit area of the sea surface, σ^0, used for the comparison (referred to as baselines curves) were obtained from various published accounts [20], [21], and [22]. These median values of the NRCS were measured at wind speeds of 4 to 6 m/s for a given elevation antenna beam-steering angle for crosswind wind direction and are identified in the legend with an "E" for experimental in each figure below.

The data used to derive the $\left\langle \left| b_{rec} / a_{trans} \right|^2 \right\rangle$ using Long, [20], are depicted in Figs. 2 and 3 with a solid-black line with squares. The curves generated from data published by Daley, et. al., [21], are shown with a dashed black line with circles and the curves generated from Plant, et. al, [22], are shown with a dashed dark-green line with inverted triangles. A similar format is employed in Figs. 4 and 5 with the addition of a different data set as provided by Long and depicted with a dashed black line with squares, and the data set generated from Plant for 6 m/s uses green lines with triangles. The data from Plant were used in Figs. 4 and 5 to confirm the trends of the simulated $\left\langle \left| b_{rec} / a_{trans} \right|^2 \right\rangle$ curves.

The code used to compute $\left\langle \left| b_{rec} / a_{trans} \right|^2 \right\rangle$ for each wave-number spectrum was initially developed in MATLAB where a method of integration derived from the 2D circular convolution was used to determine the GNRCS under the SSA. The auto-correlation function of the surface $\Re(\boldsymbol{\rho}-\boldsymbol{\rho}')$ for Figs. 2 through 5 was computed from a 2D fast-Fourier transform (FFT) of the ocean wave-number spectrum $\psi(\boldsymbol{\kappa})$ for a grid size of 2048×2048. To accelerate the calculations, the code was ported into FORTRAN 90, and the integration portion was coded using the Message Passing Interface (MPI) to take advantage of the highly parallelizable nature of the algorithm. The calculations were performed using Cray XE6's made available through the DoD Supercomputing Research Centers at the US Air Force Research Laboratory at Wright-Patterson AFB and the US Army Engineering Research and Development Center at Vicksburg, Mississippi.

The simulation curves in Fig. 2 proved to be promising for horizontal polarization, showing as little as a 4-dB deviation in the average relative received power as compared with the associated baseline values for smaller elevation angles (0° to 40°). For the larger elevation angles (50° to 75°), the deviations from the baseline relative power curve generated from Long, [20], for the Pierson-Neumann and Pierson-Moskowitz models were as large as 10 dB. The Elfouhaily model appears to provide the best overall performance with a maximum deviation of 5 dB established between baseline curves for Long, [20], and Daley, [2 1]. It should be noted that the baseline curve for Plant, [22], deviates from the remaining curves in Fig. 5. In this case, Plant's baseline would represent a lower bound on the σ^0 or $\left\langle \left| b_{rec} / a_{trans} \right|^2 \right\rangle$ values whereas the baseline values associated with the data from Long would represent an upper bound.

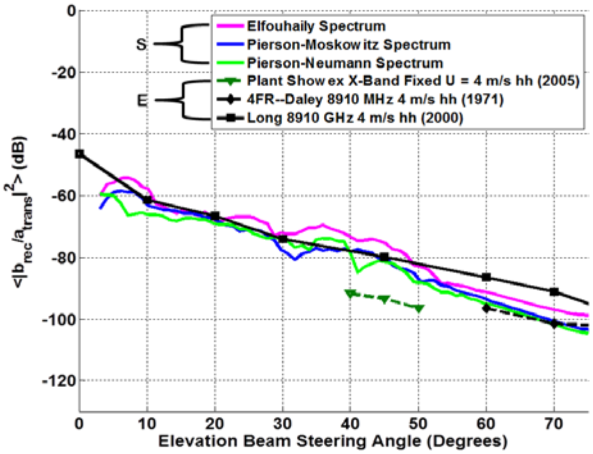

Fig. 2. Relative Received Power vs. Elevation Beam Steering Angle of a horizontally polarized circular dish above a fully developed sea surface with wind speed of 4 m/s

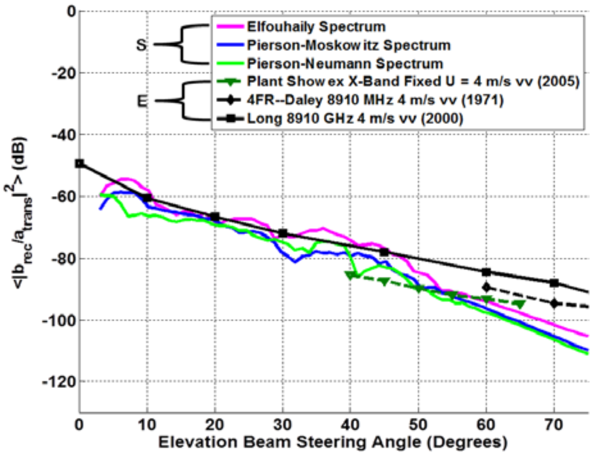

Fig. 3. Relative Received Power vs. Elevation Beam Steering Angle of a vertically polarized circular dish above a fully developed sea surface with a wind speed of 4 m/s

The results for vertical polarization shown in Fig. 3 are similar to those of Fig. 2, where the simulated $\left\langle \left| b_{rec} / a_{trans} \right|^2 \right\rangle$ curves also exhibit good agreement with the baseline curve from Long within the range of elevation angle of 0° to 40°. In re-examining Fig. 3, it is seen that there is a larger deviation from the baseline curve of Long as well, as much as 12 dB for all of the simulation curves. Again, the $\left\langle \left| b_{rec} / a_{trans} \right|^2 \right\rangle$ generated from the Elfouhaily spectrum appears to be the overall better estimate for the higher elevation angles, with a smallest 2-dB deviation compared to the lower bound and an 8-dB deviation compared to the upper bound.

The simulation curves in Fig. 4 proved to be acceptable for horizontal polarization, showing as much as a 7-dB deviation in the average relative received-power responses when compared with the associated baseline values for elevation angles of 0° to 40°. For elevation angles of 50° to 75°, the deviations were as small as 4 dB from the baseline curve generated from Long for the Pierson-Neumann and Pierson-Moskowitz models. The Elfouhaily Spectrum again provides the best overall performance with a minimum deviation of 2 dB from the baseline curve for Long and Daley. Note, the baseline curve at 4 m/s for Plant is down significantly from the remaining curves in the 50° to 75° range, by as much as 20 dB due to the partial illumination effect of the 50-ns pulse. However, Plant's curve at 6 m/s compares very well with the $\left\langle \left| b_{rec} / a_{trans} \right|^2 \right\rangle$ curves for the Pierson-Neumann and Pierson-Moskowitz models with a maximum deviation of 3 dB and the $\left\langle \left| b_{rec} / a_{trans} \right|^2 \right\rangle$ curve for the Elfouhaily Spectrum has an overall deviation of 3 dB.

The results for vertical polarization shown in Fig. 5 are also similar to those shown in Fig. 4 in that the simulated curves exhibit good agreement with the curve from Long within the range of elevation of 0° to 40°.

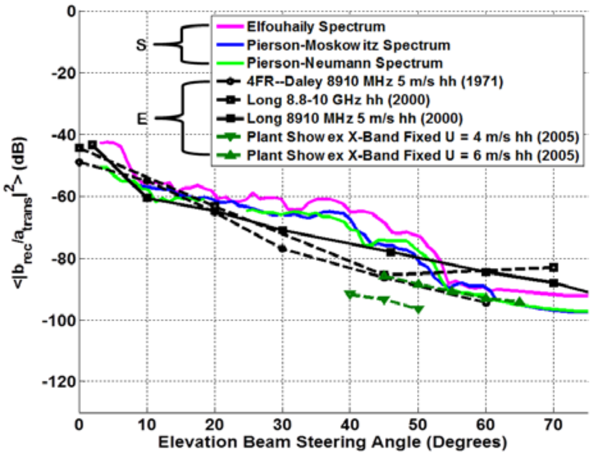

Fig. 4. Relative Received Power vs. Elevation Beam Steering Angle of a horizontally polarized circular dish above a fully developed sea surface with a wind speed of 5 m/s

In examining Fig. 5, it is seen that the larger deviation from Long's curve is as much as 7 dB for all of the simulation curves, which is due to the response within the enhanced portion. Again, the $\left\langle \left| b_{rec} / a_{trans} \right|^2 \right\rangle$ curves generated from the Elfouhaily spectrum appear to be the overall better estimate for the higher elevation angles, with a smallest 1-db deviation compared to the lower bound and a 5-dB deviation compared to the upper bound.

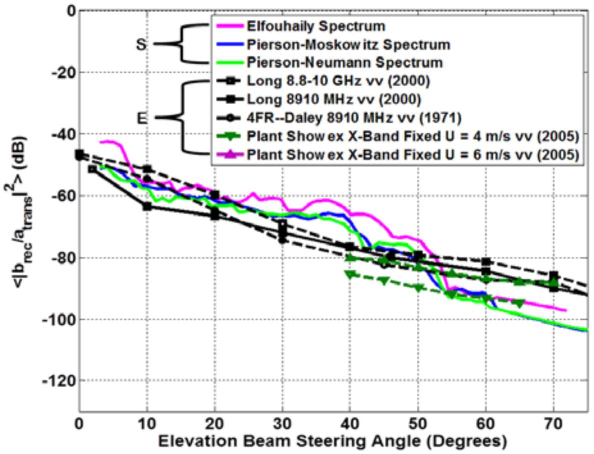

Fig. 5. Relative Received Power vs. Elevation Beam Steering Angle of a vertically polarized circular dish above a fully developed sea surface with a wind speed of 5 m/s

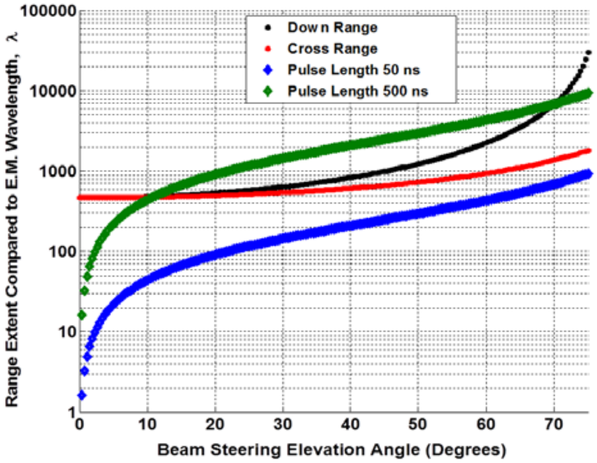

Fig. 6. Range Extent vs. Beam Steering Elevation Angles curves for the antenna footprint dimensions (cross range and down range) and pulse lengths (50 ns and 500 ns)

A special note about the simulated data is that the integration error took precedence whenever the grid spacing was not small enough (a major cause for the apparent oscillations in the curves). Another note is that for smaller angles of incidence, a few of the data points are missing, which is probably due to the queuing of the parallel processor.

VI. THE GNRCS AS A METRIC FOR SPATIAL COHERENCE

In Figs. 2 through 5, the relative power received from the sea echo, as predicted by the GNRCS, was in substantial agreement with experimental baseline values. These curves described the relationship between the surface and electromagnetic properties within the footprint. However, given the size of the footprint and the horizontal correlation lengths of sea surface, these curves were expected to converge since in most cases the footprint was limited by the antenna while the range extent associated with pulsewidth was limited by the beam's extent. Hence, the footprint consisted of sufficient number of correlation lengths such that the GNRCS was essentially identical with σ^0.

Consider Fig. 6 where the cross-range and down-range extents, and the range extents associated with two pulsewidths are shown (in terms of electromagnetic wavelengths) as a function of elevation. It can be seen where the footprint is represented by a beam-limited or pulse-limited illumination profile. The pulsewidth range extent (down-range extent) curves are shown for 500 ns and 50 ns. The 500-ns curves show that for nearly all elevation angles the footprint is beam limited, representing a fully illuminated surface for each pulse. This would mean that for the 500 ns pulse the NRCS (σ^0) is a measure of the coherence effects of the entire scattering surface defined by A. However, the 50-ns curves demonstrate that the footprint is pulse limited. Thus, the NRCS values given by Plant would signify that it was only partially illuminated, and hence the NRCS could only be defined ad hoc by the associated range extent for the appropriate angular coverage. Overall, these curves help to show that if the number of correlation lengths is sufficient to cover the antenna-beam footprint, then σ^0 is all one would need to describe the scattering nature of the surface. However, if the dimensions of A were small enough to limit the number of correlation distances within it, would σ^0 still remain a good scattering metric?

To address this question, consider the product of the gain and the back scattering cross section

$$G(\theta,\phi)\sigma(S),$$

where the $\sigma(S)$ is given by (19). If $\sigma(S)$ is replaced by σ^0, then this product would be essentially linearly proportional to the gain. Therefore, the extent to which the plots of the two products versus gain differ can be taken as a metric of the effects of spatial coherence on the backscattering cross section. In other words, if the two products are identical, then $\sigma(S)=\sigma^0$. The product

$G(\theta,\phi)\sigma(S)$ is computed in Figs. 7 and 8 at a fixed beam-center position for a circular dish when the normalized radius of the dish (k_0a) varied from 50 to 200 for a given polarization is plotted.

The $G(\theta,\phi)\sigma(S)$ curves are shown using $\sigma(S)$ obtained from the Elfouhaily Spectrum. For each polarization, the $G(\theta,\phi)\sigma^0$ curves of Daley and Long follow a linear trend. For horizontal polarization in Fig. 7, the two baseline curves are separated by 5 dB with a spread of 10 to 17 dB on the low end and 23 to 27 dB on the upper end. For gain values below 39 dB, the $G(\theta,\phi)\sigma(S)$ curve deviates substantially from the linear trend but it is nearly linear and well above the baseline curves for gain values above 39 dB.

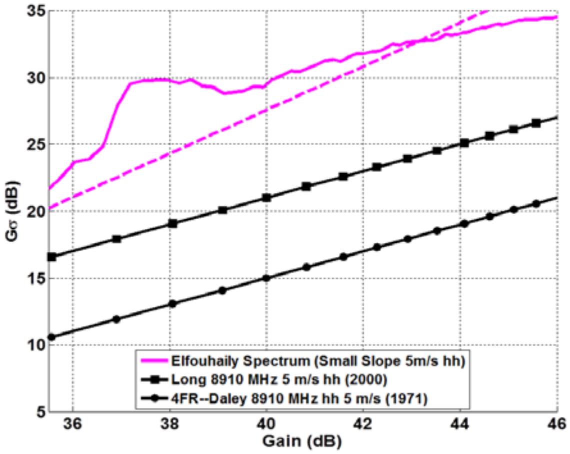

Fig. 7. The product of Gain with $\sigma(S)$ (σ^0) vs. Gain for horizontal polarization (with a wind speed of 5 m/s)

For vertical polarization in Fig. 8, the three baseline curves are separated by as much as 4 dB with a spread of 13 to 17 dB on the lower end and 23 to 28 dB on the upper end. The $G(\theta,\phi)\sigma(S)$ curve here follows a similar trend as for the horizontal polarization. Both of these figures show that as the gain increases, or the antenna-footprint dimensions decrease, $G(\theta,\phi)\sigma^0$ increases linearly. However, the $G(\theta,\phi)\sigma(S)$ curve has a non-linear trend that is well above the upper-bound baseline curve, which implies that the scattering crossing section is gain dependent. Hence, the number of horizontal spatial correlation lengths establishes the relative strength of the backscattered field. This demonstrates that the GNRCS is the best metric for characterizing radar clutter.

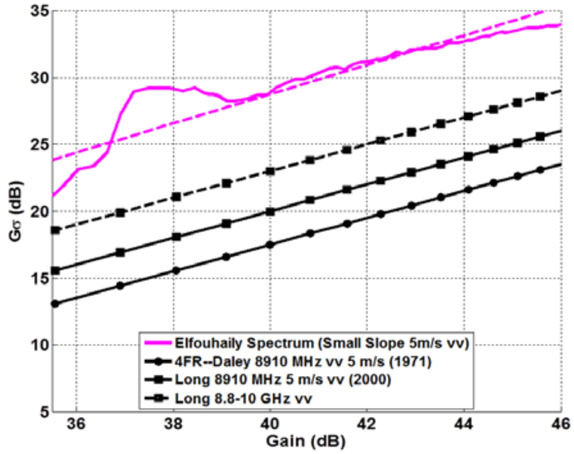

Fig. 8. The product of Gain with $\sigma(S)$ (σ^0) vs. Gain for vertical polarization (with a wind speed of 5 m/s)

VII. CONCLUSIONS

The coherence effects on the backscattered field due to a random sea surface, as established by the properties of the radiating antenna, were investigated using the antenna-reciprocity relationship to predict the mono-static signal returns from beam-resolved distributed targets for sea-clutter analysis. The sea-surface backscatter was examined for a fully developed wind-driven sea modeled by several empirical wave-number spectra in the presence of a uniformly illuminated circular dish at X-band. The relative power returns were determined for various antenna parameters (height above surface, polarization, and beam footprint) for a given sea state. The relative-power curves generated by the GNRCS compared very well with responses derived from measured data. The deviations obtained from the data-derived baseline trends were as small as 3 dB. Oddly enough, the simulated responses performed unexpectedly well at the high-incidence angles, a major indication that rough-surface scattering analysis should include the full nature of the incident field as well the surface kinematics. Overall, the results show that spatial-coherence effects can significantly influence radar-clutter estimates.

A special note about the simulated data, which was previously mentioned, is that the integration error took precedence whenever the grid spacing was not small enough, which is a major cause for the apparent oscillations in the curves.

ACKNOWLEDGEMENTS

The authors would like to thank the reviewers for their insightful comments. Also, the authors would to like thank the U.S. Naval Research Laboratory (especially the radar division) for allowing us to use the HPMCP computers to run these extensive simulations for the paper. Finally, the authors would like to extend a major debt of gratitude to Dr. C. Kung for assisting us in translating the MATLAB code into FORTRAN 90 and for establishing us on the HPMCP environment.

REFERENCES

[1] M.I. Skolnik, *Radar Handbook*: McGraw-Hill, 2008.

[2] G. Berginc, "Small-slope approximation method: A further study of vector wave scattering from two-dimensional surfaces and comparison with experimental data," *Progress in Electromagnetics Research,* vol. 37, pp. 251-287, 2002.

[3] O.M. Phillips, "Radar return from the sea surface - Bragg scattering and breaking waves," *Journal of Fluid Mechanics,* vol. 156, pp. 505-531, 1988.

[4] W.J. Plant, "A stochastic, multiscale model of microwave backscatter from the ocean," *Journal of Geophysical Research C: Oceans,* vol. 107, pp. 3-1, 2002.

[5] W.J. Plant, P.H. Dahl, and W.C. Keller, "Microwave and acoustic scattering from parasitic capillary waves," *Journal of Geophysical Research C: Oceans,* vol. 104, pp. 25853-25866, 1999.

[6] D. Holliday, L.L. DeRaad, and G.J. St-Cyr, "Forward-backward: a new method for computing low-grazing angle scattering," *Antennas and Propagation, IEEE Transactions on,* vol. 44, pp. 722--722, 1996.

[7] D. Holliday, L.L. DeRaad, Jr., and G.J. St-Cyr, "Sea-spike backscatter from a steepening wave," *Antennas and Propagation, IEEE Transactions on,* vol. 46, pp. 108-113, January 1998.

[8] W. Wasylkiwskyj, "A new formulation for coherent backscattering from distributed targets," *IEEE Antennas and Propagation Society International Symposium*, Honolulu, HI; pp. 5693 - 5696, June 2007.

[9] J.W. Wright and W.C. Keller, "Doppler spectra in microwave scattering from wind waves," *Physics of Fluids,* vol. 14, pp. {466-\&}, 1971.

[10] D.M. Levine, "Comparison of σ^0 Obtained from the Conventional Definition with σ^0 Appearing in the Radar Equation for Randomly Rough Surfaces," *IEEE Transactions on Geoscience and Remote Sensing,* vol. GE-20, pp. 85-90, 1982.

[11] D. Holliday, G. St-Cyr, and N.E. Woods, "A radar ocean imaging model for small to moderate incidence angles," *International Journal of Remote Sensing,* vol. 7, pp. 1809-1834, 1986.

[12] W. Wasylkiwskyj and J. Alatishe, "Coherent scattering from distributed targets," *Microwaves, Radar and Remote Sensing Symposium*, Kiev, Ukraine; pp. 36-41, September 2008.

[13] W. Wasylkiwskyj, "Gain, Efficiency, and Receiving Cross Section of Antennas in a Dissipative Medium," *Radio Science,* vol. 5, pp. 1361-1374, 1970.

[14] W. Wasylkiwskyj and W.K. Kahn, "Theory of mutual coupling among minimum-scattering antennas," *IEEE Transactions on Antennas and Propagation,* vol. 18, pp. 204-216, 1970.

[15] A.C. Gately, Jr., D.J.R. Stock, and B. R. Cheo, "A network description for antenna problems," *Proceedings of the IEEE,* vol. 56, pp. 1181-1193, 1968.

[16] A.G. Voronvich, *Wave scattering from rough surfaces*, 2 ed.: Springer, 1999.

[17] T. Elfouhaily, B. Chapron, K. Katsaros, and D. Vandemark, "A unified directional spectrum for long and short wind-driven waves," *Journal of Geophysical Research,* vol. 102, pp. 15781-15796, 15 1997.

[18] B. Kinsman, *Wind Waves, Their Generation and Propagation on the Ocean Surface*: Prentice-Hall, 1965.

[19] W.J. Pierson and L. Moskowitz, "Proposed Spectral Form for Fully Developed Wind Seas Based on Similarity Theory of S a Kitaigorodskii," *Journal of Geophysical Research,* vol. 69, pp. 5181-&amp;, 1964.

[20] M.W. Long, *Radar Reflectivity of Land and Sea*: Artech House, 2001.

[21] J.C. Daley, J.T. Ransone, and J.A. Burkett, "Radar Sea Return - JOSS I," NRL, UP DEPT OF COMMERCE, SPRINGFIELD, VA 22161, Formal Report APR 1971.

[22] W.J. Plant, W.C. Keller, and K. Hayes, "Simultaneous measurement of ocean winds and waves with an airborne coherent real aperture radar," *Journal of Atmospheric and Oceanic Technology,* vol. 22, pp. 832-846, 2005.

[23] W. Wasylkiwskyj, "Response of an antenna to arbitrary incident fields," *IEEE Antennas and Propagation Society International Symposium*, Washington , DC; pp. 39-42vol. 3B, July 2005.

[25] A.G. Voronovich, "A two-scale model from the point of view of the small-slope approximation," *Waves in Random Media,* vol. 6, pp. 73-83, 1996.

[26] G.R. Valenzuela, "Theories for the interaction of electromagnetic and oceanic waves - A review," *Boundary-Layer Meteorology,* vol. 13, pp. 61-85, 1978.

APPENDIX A

DERIVATION OF THE ANTENNA RESPONSE FROM A FIELD SCATTERED BY AN IRREGULAR DIELECTRIC /AIR INTERFACE USING A MODIFIED VERSION OF THE SSA

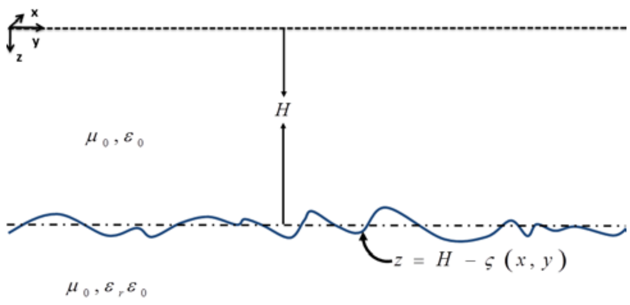
x
y
z
H
μ_0, ε_0
$z = H - \varsigma(x, y)$
$\mu_0, \varepsilon_r \varepsilon_0$

Fig. A1. Description of the scattering media

The bounding surface between the dielectric medium and free space in Fig. A1 is defined with respect to the reference plane H by $H - \varsigma(x, y)$. The free-space and dielectric regions correspond, respectively, to $z \le H - \min \varsigma(x, y)$ and $z \ge H - \max \varsigma(x, y)$. A plane wave $\mathbf{E}_i e^{-j\mathbf{k}_{ti}\cdot\boldsymbol{\rho} - jk_{zi}z}$, incident from free space together with the outgoing waves, is represented by

$$\mathbf{E}(\mathbf{r}) = \mathbf{E}_i e^{-j\mathbf{k}_{ti}\cdot\boldsymbol{\rho} - jk_{zi}z} + \mathbf{E}_{refl} e^{-j\mathbf{k}_{ti}\cdot\boldsymbol{\rho} + jk_{zi}(z-2H)} + e^{-jk_{zi}H}\int d^2\mathbf{k}_t \mathbb{E}_s(\mathbf{k}_t, \mathbf{k}_{ti}) e^{-j\mathbf{k}_t\cdot\boldsymbol{\rho} + jk_z(z-H)}. \tag{A1}$$

In accordance with the Rayleigh hypothesis, the last term, represented by the Fourier integral, and referenced to the plane $z = H$, is an approximation to the continuous spectrum and is defined as the scattered field, excluding the specular term $\mathbf{E}_{refl} e^{-j\mathbf{k}_{ti}\cdot\boldsymbol{\rho} + jk_{zi}(z-2H)}$. The electric field transmitted into the dielectric region is

$$\mathbf{E}^{(2)}(\mathbf{r}) = \mathbf{E}_{refr} e^{-jk_{zi}H} e^{-j\mathbf{k}_{ti}\cdot\boldsymbol{\rho} - jk_{2zi}(z-H)} + e^{-jk_{zi}H}\int d^2\mathbf{k}_t \mathbb{E}_s^{(2)}(\mathbf{k}_t, \mathbf{k}_{ti}) e^{-j\mathbf{k}_t\cdot\boldsymbol{\rho} - jk_{2z}(z-H)}, \tag{A2}$$

and similarly for the corresponding magnetic fields $\mathbf{H}(\mathbf{r})$ and $\mathbf{H}^{(2)}(\mathbf{r})$. $\mathbb{E}_s(\mathbf{k}_t, \mathbf{k}_{ti})$ and $\mathbb{E}_s^{(2)}(\mathbf{k}_t, \mathbf{k}_{ti})$ are electric-field scattering amplitudes, respectively, in air and the dielectric medium. The following is an outline of the procedure used to find an approximate solution to (A1) for $\mathbb{E}(\mathbf{k}_t, \mathbf{k}_{ti})$ (essentially a Taylor expansion to $O|\nabla_t\varsigma|$) and relate it to the generalized NRCS, which is one of the objectives of the paper under review.

The symbols indicated here and in the subsequent equations are defined as follows: $\mathbf{k}_t$ is the transverse wave number (i.e., the projection of the wave number $\mathbf{k}$ on the xy plane); k_z and k_{2z} are z-components of $\mathbf{k}$, respectively, in air and the dielectric medium; k_0 is the free-space wave number; subscript i refers to quantities associated with incident fields, subscript t to transverse components; $\boldsymbol{\kappa}_{01} = \frac{\mathbf{k}_t}{k_0}$ and $\boldsymbol{\kappa}_{02} = \mathbf{z}_0 \times \boldsymbol{\kappa}_{01}$ are unit vectors along the x and y axes, $\boldsymbol{\rho}$ is the position vector in the xy plane, and $Z_0 = \sqrt{\frac{\mu_0}{\varepsilon_0}}$.

Matching the six tangential components of the total electric and magnetic fields on the media bounding surface and, independently, the tangential components of the plane wave on the hypothetical planar boundary H, yields the following set of integral equations for the scattering amplitudes

$$\begin{bmatrix} \mathbb{E}_s(\mathbf{k}_t, \mathbf{k}_{ti}) \\ \mathbb{E}_s^{(2)}(\mathbf{k}_t, \mathbf{k}_{ti}) \end{bmatrix} = \int d^2\mathbf{k}_t' \begin{bmatrix} \mathbf{K}_{11}(\mathbf{k}_t, \mathbf{k}_t') & \mathbf{K}_{12}(\mathbf{k}_t, \mathbf{k}_t') \\ \mathbf{K}_{21}(\mathbf{k}_t, \mathbf{k}_t') & \mathbf{K}_{22}(\mathbf{k}_t, \mathbf{k}_t') \end{bmatrix} \begin{bmatrix} \mathbb{E}_s(\mathbf{k}_t', \mathbf{k}_{ti}) \\ \mathbb{E}_s^{(2)}(\mathbf{k}_t', \mathbf{k}_{ti}) \end{bmatrix} + \begin{bmatrix} \mathbf{V}_1(\mathbf{k}_t, \mathbf{k}_{ti}) \\ \mathbf{V}_2(\mathbf{k}_t, \mathbf{k}_{ti}) \end{bmatrix}, \tag{A3}$$

where the matrix elements $\mathbf{K}_{mn}(\mathbf{k}_t, \mathbf{k}_t')$ are 3x3 dyadics that depend on wave numbers, the surface slope, and plane-wave Fresnel coefficients. Upon applying the Neumann iteration procedure to (A3) one finds that to represent the solution to within $O(|\nabla\varsigma|)$ the first term suffices. This is equivalent to approximating $\mathbb{E}_s(\mathbf{k}_t, \mathbf{k}_{ti})$ by $\mathbf{V}_1(\mathbf{k}_t, \mathbf{k}_{ti})$ in (A3), which is (it is important to note this approximation does not constrain the size of $|k_0\varsigma|$)

$$\mathbb{E}_s(\mathbf{k}_t, \mathbf{k}_{ti}) = \mathbf{T}_E^{(1)} \cdot \mathbf{V}_E(\mathbf{k}_t, \mathbf{k}_{ti}) + \mathbf{T}_H^{(1)} \cdot \mathbf{V}_H(\mathbf{k}_t, \mathbf{k}_{ti}); \tag{A4}$$

where

$$\mathbf{T}_E^{(1)}(\mathbf{k}_t) = \left[\frac{-k_z\varepsilon_r}{k_z\varepsilon_r + k_{2z}}\boldsymbol{\kappa}_{01}\boldsymbol{\kappa}_{02} + \frac{k_z}{k_z + k_{2z}}\boldsymbol{\kappa}_{02}\boldsymbol{\kappa}_{01} - \frac{k_t\varepsilon_r}{k_z\varepsilon_r + k_{2z}}\mathbf{z}_0\boldsymbol{\kappa}_{02}\right], \tag{A5}$$

and

$$\mathbf{T}_H^{(1)}(\mathbf{k}_t) = \left[\frac{-k_z k_{2z}}{k_0^2(k_z\varepsilon_r + k_{2z})}\boldsymbol{\kappa}_{01}\boldsymbol{\kappa}_{01} + \frac{1}{k_z + k_{2z}}\boldsymbol{\kappa}_{02}\boldsymbol{\kappa}_{02} - \frac{k_t k_{2z}}{k_0^2(k_z\varepsilon_r + k_{2z})}\mathbf{z}_0\boldsymbol{\kappa}_{01}\right]; \tag{A6}$$

and

$$\mathbf{V}_E(\mathbf{k}_t, \mathbf{k}_{ti}) = \frac{-1}{(2\pi)^2}\int d^2\rho\, e^{j(\mathbf{k}_t - \mathbf{k}_{ti})\cdot\boldsymbol{\rho}} \cdot \left\{ \begin{matrix} (\mathbf{E}_i \times \mathbf{z}_0) e^{jk_{zi}\varsigma(x,y)} + (\mathbf{E}_{refl} \times \mathbf{z}_0) e^{-jk_{zi}\varsigma(x,y)} \\ -(\mathbf{E}_{refr} \times \mathbf{z}_0) e^{-jk_{2zi}\varsigma(x,y)} \end{matrix} \right\} \tag{A7}$$

and

$$\mathbf{V}_H\left(\mathbf{k}_t,\mathbf{k}_{ti}\right)=\frac{-k_oZ_o}{(2\pi)^2}\int d^2\boldsymbol{\rho}e^{j(\mathbf{k}_t-\mathbf{k}_{ti})\cdot\boldsymbol{\rho}}\left\{\begin{array}{c}\left(\mathbf{z}_0\times\mathbf{H}_i\right)e^{jk_{zi}\varsigma(x,y)}+\left(\mathbf{z}_0\times\mathbf{H}_{refl}\right)e^{-jk_{zi}\varsigma(x,y)}\\ -\left(\mathbf{z}_0\times\mathbf{H}_{refr}\right)e^{jk_{2zi}\varsigma(x,y)}\end{array}\right\}. \tag{A8}$$

Recasting this in spherical coordinates, we denote the angles of incidence by θ_i (elevation), and ϕ_i (azimuth) and the scattering angles by α and β, the electric-field scattering amplitude resolved along the spherical unit vectors $\boldsymbol{\alpha}_0$ and $\boldsymbol{\beta}_0$ assumes the form

$$\mathbb{E}_s\left(\mathbf{k}_t,\mathbf{k}_{ti}\right)=\int d^2\boldsymbol{\rho}e^{j\left(\mathbf{k}_t^{'}-\mathbf{k}_{ti}\right)\cdot\boldsymbol{\rho}}\boldsymbol{\Psi}\left(\mathbf{k}_t,\mathbf{k}_{ti},\boldsymbol{\rho}\right); \tag{A9}$$

where

$$\boldsymbol{\Psi}\left(\mathbf{k}_t,\mathbf{k}_{ti},\boldsymbol{\rho}\right)=\left\{\boldsymbol{\alpha}_o\left[T_{\alpha\theta_i}E_{i\theta}+T_{\alpha\varphi_i}E_{i\varphi}\right]+\boldsymbol{\beta}_o\left[T_{\beta\theta_i}E_{i\theta}+T_{\beta\varphi_i}E_{i\varphi}\right]\right\}, \tag{A10}$$

and

$$T_{\alpha\theta_i}\left(\mathbf{k}_t,\mathbf{k}_{ti},\boldsymbol{\rho}\right)=\frac{\cos\left(\beta-\phi_i\right)}{(2\pi)^2\left(\sqrt{\varepsilon_r-\sin^2\alpha}+\varepsilon_r\cos\alpha\right)}\bullet$$
$$\left\{\begin{array}{l}\left[\varepsilon_r\cos\theta_i-\sqrt{\varepsilon_r-\sin^2\alpha}\right]\left(e^{jk_{zi}\varsigma(\boldsymbol{\rho})}-e^{-jk_{2zi}\varsigma(\boldsymbol{\rho})}\right)\\ +\left[\varepsilon_r\cos\theta_i+\sqrt{\varepsilon_r-\sin^2\alpha}\right]\Gamma'\left(\theta_i\right)\left(e^{-jk_{zi}\varsigma(\boldsymbol{\rho})}-e^{-jk_{2zi}\varsigma(\boldsymbol{\rho})}\right)\end{array}\right\} \tag{A11}$$

$$T_{\alpha\phi_i}\left(\mathbf{k}_t,\mathbf{k}_{ti},\boldsymbol{\rho}\right)=\frac{\sin\left(\beta-\phi_i\right)}{(2\pi)^2\left(\sqrt{\varepsilon_r-\sin^2\alpha}+\varepsilon_r\cos\alpha\right)}\bullet$$
$$\left\{\begin{array}{l}\left[\varepsilon_r-\sqrt{\varepsilon_r-\sin^2\alpha}\cos\theta_i\right]\left(e^{jk_{zi}\varsigma(\boldsymbol{\rho})}-e^{jk_{2zi}\varsigma(\boldsymbol{\rho})}\right)\\ +\left[\varepsilon_r+\sqrt{\varepsilon_r-\sin^2\alpha}\cos\theta_i\right]\Gamma''\left(\theta_i\right)\left(e^{-jk_{zi}\varsigma(\boldsymbol{\rho})}-e^{jk_{2zi}\varsigma(\boldsymbol{\rho})}\right)\end{array}\right\} \tag{A12}$$

$$T_{\beta\theta_i}\left(\mathbf{k}_t,\mathbf{k}_{ti},\boldsymbol{\rho}\right)=\frac{-\sin\left(\beta-\phi_i\right)}{(2\pi)^2\left(\sqrt{\varepsilon_r-\sin^2\alpha}+\cos\alpha\right)}\bullet$$
$$\left\{\begin{array}{l}\left[1-\sqrt{\varepsilon_r-\sin^2\alpha}\cos\theta_i\right]\left(e^{jk_{zi}\varsigma(\boldsymbol{\rho})}-e^{jk_{2zi}\varsigma(\boldsymbol{\rho})}\right)\\ +\left[1+\sqrt{\varepsilon_r-\sin^2\alpha}\cos\theta_i\right]\Gamma'\left(\theta_i\right)\left(e^{-jk_{zi}\varsigma(\boldsymbol{\rho})}-e^{jk_{2zi}\varsigma(\boldsymbol{\rho})}\right)\end{array}\right\} \tag{A13}$$

$$T_{\beta\phi_i}\left(\mathbf{k}_t,\mathbf{k}_{ti},\boldsymbol{\rho}\right)=\frac{-\cos\left(\beta-\phi_i\right)}{(2\pi)^2\left(\sqrt{\varepsilon_r-\sin^2\alpha}+\cos\alpha\right)}\bullet$$
$$\left\{\begin{array}{l}\left[\sqrt{\varepsilon_r-\sin^2\alpha}-\cos\theta_i\right]\left(e^{jk_{zi}\varsigma(\boldsymbol{\rho})}-e^{-jk_{2zi}\varsigma(\boldsymbol{\rho})}\right)\\ +\left[\sqrt{\varepsilon_r-\sin^2\alpha}+\cos\theta_i\right]\Gamma''\left(\theta_i\right)\left(e^{-jk_{zi}\varsigma(\boldsymbol{\rho})}-e^{-jk_{2zi}\varsigma(\boldsymbol{\rho})}\right)\end{array}\right\}. \tag{A14}$$

Next we consider the reception of the scattered field by an antenna. From the generalized reciprocity relationship [23] we have

$$a_{trans}b_{rec}=\frac{-j}{2\pi k_0\sqrt{Z_0}}\int\mathbf{F}_{rad}\left(\mathbf{k}_t^{'}\right)\cdot\widetilde{\mathbf{E}}\left(\mathbf{k}_t^{'}\right)d^2\mathbf{k}_t^{'}. \tag{A15}$$

With this normalization $\left|b_{rec}\right|^2$ is the received power, and the electric far field on transmission is

$$\sqrt{Z_0}\,\frac{\mathbf{F}_{rad}\left(\mathbf{k}_t^{'}\right)}{R}e^{-jk_0R}, \tag{A16}$$

with the corresponding radiated power

$$\iint_{4\pi}\left|\mathbf{F}_{rad}\left(\mathbf{k}_t^{'}\right)\right|^2\left(\frac{d^2\mathbf{k}_t^{'}}{k_0^2\cos\theta}\right)\propto\left|a_{trans}\right|^2. \tag{A17}$$

For compatibility with these definitions $\widetilde{\mathbf{E}}\left(\mathbf{k}_t^{'}\right)$ represents the Fourier Transform of the scattered field at $z=0$, i.e.,

$$\widetilde{\mathbf{E}}\left(\mathbf{k}_t^{'}\right)=\int\mathbf{E}_s\left(\boldsymbol{\rho},0\right)e^{-j\mathbf{k}_t^{'}\cdot\boldsymbol{\rho}}d^2\boldsymbol{\rho}. \tag{A18}$$

To use formula (A15) we must express $\widetilde{\mathbf{E}}\left(\mathbf{k}_t^{'}\right)$ in terms of the scattering amplitude $\mathbb{E}_s\left(\mathbf{k}_t,\mathbf{k}_{ti}\right)$ in (A1). For a single incident spectral component (i.e., a plane wave)

$$\widehat{\mathbf{E}}_s\left(\mathbf{k}_{ti},\boldsymbol{\rho},z,\right)=e^{-jk_{zi}H}\iint d^2\mathbf{k}_t^{'}\mathbb{E}_s\left(\mathbf{k}_t^{'},\mathbf{k}_{ti}\right)e^{-j\mathbf{k}_t^{'}\cdot\boldsymbol{\rho}}e^{-jk_z^{'}(z-H)}. \tag{A19}$$

For a general illumination we need

$$\mathbf{E}_s\left(\boldsymbol{\rho},0\right)=\frac{1}{(2\pi)^2}\int\widehat{\mathbf{E}}_s\left(\mathbf{k}_{ti},\boldsymbol{\rho},0,\right)d^2\mathbf{k}_{ti}, \tag{A20}$$

which is restricted to the plane $z=0$, the location of the antenna. Substituting (A20) in (A18) we get

$$\begin{aligned}\widetilde{\mathbf{E}}\left(\mathbf{k}_t^{'}\right)&=\frac{1}{(2\pi)^2}\iiint\mathbb{E}_s\left(\mathbf{k}_t,\mathbf{k}_{ti}\right)e^{-j(k_{zi}+k_z)H}e^{-j\left(\mathbf{k}_t+\mathbf{k}_t^{'}\right)\cdot\boldsymbol{\rho}}d^2\boldsymbol{\rho}d^2\mathbf{k}_td^2\mathbf{k}_{ti}\\ &=\iint\mathbb{E}_s\left(\mathbf{k}_t,\mathbf{k}_{ti}\right)e^{-j(k_{zi}+k_z)H}\delta\left(\mathbf{k}_t+\mathbf{k}_t^{'}\right)d^2\mathbf{k}_td^2\mathbf{k}_{ti}\\ &=\int\mathbb{E}_s\left(-\mathbf{k}_t^{'},\mathbf{k}_{ti}\right)e^{-j\left(k_{zi}+k_z^{'}\right)H}d^2\mathbf{k}_{ti}.\end{aligned} \tag{A21}$$

Substituting the last expression in (A19) we get the receiver output in terms of the spatial spectrum:

$$a_{trans}b_{rec}=\frac{-j\int\mathbf{F}_{rad}\left(\mathbf{k}_t^{'}\right)\cdot\left[\int d^2\mathbf{k}_{ti}\mathbb{E}_s\left(-\mathbf{k}_t^{'},\mathbf{k}_{ti}\right)e^{-j\left(k_{zi}+k_z^{'}\right)H}\right]d^2\mathbf{k}_t^{'}}{2\pi k_o\sqrt{Z_o}}. \tag{A22}$$

A form more suitable for stationary phase evaluation is obtained by replacing $\mathbb{E}_s\left(-\mathbf{k}_t^{'},\mathbf{k}_{ti}\right)$ in (A22) with (A9)

$$a_{trans}b_{rec}=\frac{-j\int d^2\boldsymbol{\rho}\iint \mathbf{F}_{rad}\left(\mathbf{k}_t^{'}\right)\cdot\boldsymbol{\Psi}\left(-\mathbf{k}_t^{'},\mathbf{k}_{ti},\boldsymbol{\rho}\right)e^{-j\mathbf{k}\cdot\mathbf{R}}e^{-j\mathbf{k}^{'}\cdot\mathbf{R}}d^2\mathbf{k}_{ti}d^2\mathbf{k}_t^{'}.}{2\pi k_o\sqrt{Z_o}}\tag{A23}$$

For $k_0R\gg 1$ ((A20) is good enough) we can use stationary phase, one corresponding to $e^{-j\mathbf{k}^{'}\cdot\mathbf{R}}$ the other to $e^{-j\mathbf{k}\cdot\mathbf{R}}$ with stationary points at $\alpha=\theta$, $\beta=\phi$, and $\theta_i=\theta$, $\phi_i=\phi$. This translates into $\mathbf{k}_t=\mathbf{k}_{ti}=\boldsymbol{\rho}_0k_0\sin\theta$ and in (A9) $\boldsymbol{\alpha}_0=-\boldsymbol{\theta}_0$, $\boldsymbol{\beta}_0=-\boldsymbol{\phi}_0$. As result we get

$$a_{trans}b_{rec}=\frac{-j\int d^2\boldsymbol{\rho}\cos^2\theta\frac{e^{-j2k_0R}}{R^2}\mathbf{F}_{rad}\left(\mathbf{k}_t^{'}\right)\cdot\boldsymbol{\Psi}\left(-\boldsymbol{\rho}_0k_0\sin\theta,\boldsymbol{\rho}_0k_0\sin\theta,\boldsymbol{\rho}\right)}{2\pi k_0\sqrt{Z_0}}.\tag{A24}$$

The matrix elements in (A11), (A12), (A13), and (A14) evaluated at the stationary points are:

$$\begin{aligned}
T_{\alpha\theta_i}\left(-\mathbf{k}_t^{'},\mathbf{k}_{ti},\boldsymbol{\rho}\right)&=\frac{2j}{(2\pi)^2}\Gamma'(\theta)\sin\left[k_0\varsigma(\boldsymbol{\rho})\cos\theta\right];\\
T_{\beta\phi_i}\left(-\mathbf{k}_t^{'},\mathbf{k}_{ti},\boldsymbol{\rho}\right)&=-\frac{2j}{(2\pi)^2}\Gamma''(\theta)\sin\left[k_0\varsigma(\boldsymbol{\rho})\cos\theta\right];\\
T_{\beta\theta_i}\left(-\mathbf{k}_t^{'},\mathbf{k}_{ti},\boldsymbol{\rho}\right)&=T_{\alpha\phi_i}\left(-\mathbf{k}_t^{'},\mathbf{k}_{ti},\boldsymbol{\rho}\right)=0,
\end{aligned}\tag{A25}$$

so that

$$\begin{aligned}
&\boldsymbol{\Psi}\left(-\boldsymbol{\rho}_0k_0\sin\theta,\boldsymbol{\rho}_0k_0\sin\theta,\boldsymbol{\rho}\right)=\\
&\frac{2j}{(2\pi)^2}\sin\left[k_0\varsigma(\boldsymbol{\rho})\cos\theta\right]\left\{-\boldsymbol{\theta}_0\Gamma'(\theta)E_{i\theta}+\boldsymbol{\phi}_0\Gamma''(\theta)E_{i\phi}\right\}.
\end{aligned}\tag{A26}$$

Here as in (A9) $E_{i\theta}$ and $E_{i\phi}$ are proportional to $F_{rad\theta}$ and $F_{rad\phi}$, the components of $\mathbf{F}_{rad}\left(\mathbf{k}_t^{'}\right)$ in (A16). We can find the proportionality constants by recognizing that (A16) is the asymptotic form of the electric field $\mathbf{E}_{rad}(\mathbf{R})$ as $k_0R\to\infty$ that can be computed from

$$\mathbf{E}_{rad}(\mathbf{R})=\frac{1}{(2\pi)^2}\int\widetilde{\mathbf{E}}_i\left(\mathbf{k}_t\right)e^{-j\mathbf{k}\cdot\mathbf{R}}d^2\mathbf{k}_t.\tag{A27}$$

A stationary phase evaluation gives

$$\begin{aligned}
\mathbf{E}_{rad}(\mathbf{R})&\sim\frac{k_0^2}{(2\pi)^2}\left(\frac{2\pi j}{k_0R}\right)e^{-jk_0R}\cos\theta\widetilde{\mathbf{E}}_i(\theta,\varphi)\\
&\equiv\sqrt{Z_0}\frac{\mathbf{F}_{rad}(\theta,\varphi)}{R}e^{-jk_0R}.
\end{aligned}\tag{A28}$$

Writing (A28) in component form

$$\boldsymbol{\theta}_0F_{rad\theta}+\boldsymbol{\phi}_0F_{rad\phi}=\frac{k_0^2}{\sqrt{Z_0}(2\pi)^2}\left(\frac{2\pi j}{k_0}\right)\cos\theta\left(\boldsymbol{\theta}_0E_{i\theta}+\boldsymbol{\phi}_0E_{i\phi}\right),\tag{A29}$$

we obtain the desired proportionality constants:

$$E_{i\theta}=\frac{\sqrt{Z_0}2\pi F_{rad\theta}}{jk_0\cos\theta},E_{i\phi}=\frac{\sqrt{Z_0}2\pi F_{rad\phi}}{jk_0\cos\theta}\tag{A30}$$

Using these in (A26),

$$\begin{aligned}
&\boldsymbol{\Psi}\left(-\boldsymbol{\rho}_0k_0\sin\theta,\boldsymbol{\rho}_0k_0\sin\theta,\boldsymbol{\rho}\right)=\frac{\sqrt{Z_0}\sin\left[k_0\varsigma(\boldsymbol{\rho})\cos\theta\right]}{\pi k_0\cos\theta}\\
&\cdot\left\{-\boldsymbol{\theta}_0\Gamma'(\theta)F_{rad\theta}+\boldsymbol{\phi}_0\Gamma''(\theta)F_{rad\phi}\right\}.
\end{aligned}\tag{A31}$$

The final form of the receiver output is obtained by the substitution of (A31) into (A24)

$$\begin{aligned}
a_{trans}b_{rec}&=j2\pi\int d^2\boldsymbol{\rho}\cos\theta\frac{e^{-j2k_0R}}{R^2}\frac{\sin\left[k_0\varsigma(\boldsymbol{\rho})\cos\theta\right]}{\pi}\mathbf{F}_{rad}(\theta,\phi)\cdot\left[-\boldsymbol{\theta}_0\Gamma'(\theta)F_{rad\theta}+\boldsymbol{\phi}_0\Gamma''(\theta)F_{rad\phi}\right]\\
&=-j\frac{2\pi}{k_0}\int d^2\boldsymbol{\rho}\frac{e^{-j2k_0R}}{R^2}\frac{k_0\cos\theta}{\pi}\sin\left[k_0\varsigma(\boldsymbol{\rho})\cos\theta\right]\left\{\boldsymbol{\theta}_0\Gamma'(\theta)F_{rad\theta}^2-\boldsymbol{\phi}_0\Gamma''(\theta)F_{rad\phi}^2\right\},
\end{aligned}\tag{A32}$$

or

$$\begin{aligned}
a_{trans}b_{rec}&=-j\frac{2\pi}{k_0}\int d^2\boldsymbol{\rho}\frac{e^{-j2k_0R}}{R^2}\frac{k_0\cos\theta}{\pi}\sin\left[k_0\varsigma(\boldsymbol{\rho})\cos\theta\right]\begin{bmatrix}F_{rad\theta}\\F_{rad\phi}\end{bmatrix}^T\begin{bmatrix}\Gamma'(\theta)&0\\0&-\Gamma''(\theta)\end{bmatrix}\begin{bmatrix}F_{rad\theta}\\F_{rad\phi}\end{bmatrix}\\
&=-j\frac{2\pi}{k_0}\int d^2\boldsymbol{\rho}\frac{e^{-j2k_0R}}{R^2}\mathbf{F}_{rad}(\theta,\phi)\cdot\mathbf{S}_{distr}(\theta,\phi)\cdot\mathbf{F}_{rad}(\theta,\phi)
\end{aligned}\tag{A33}$$

APPENDIX B

BRIEF DERIVATION OF THE ROUGH- SURFACE FIELD INTEGRAL EQUATION FOR THE MODIFIED SAA

A synopsis of the derivation of some of the key formulas used to obtain the integral equations given in Appendix A and the scattering matrix given in (9) of the paper are explained herein. The formalism given in Appendix A will be adopted in this document. We wish to emphasize that the formulation in our paper is an alternate version to the formulation given in [16], although ours renders substantially different expressions with unique functional properties. The differences in the expressions are primarily due to the application of the surface constraints for small slope $\left|\nabla_t\varsigma(x,y)\right|\ll 1$ and small amplitude $\left|k_0\varsigma(x,y)\right|\ll 1$, and the phase reference associated with the mean surface displacement (which will be explained in the sequel). The methodology presented in [16] and [25], and summarized in [26] utilizes the surface constraints simultaneously for the SSA. However, the formulation given in Section VIII and herein, employ these constraints separately.

Herein, the approximate form of the rough-surface scattered field is obtained by a construction that assumes the validity of the Rayleigh hypothesis (See Fig. B1). Beginning with the description of the aforementioned construction of the electromagnetic fields in both media, we have the following.

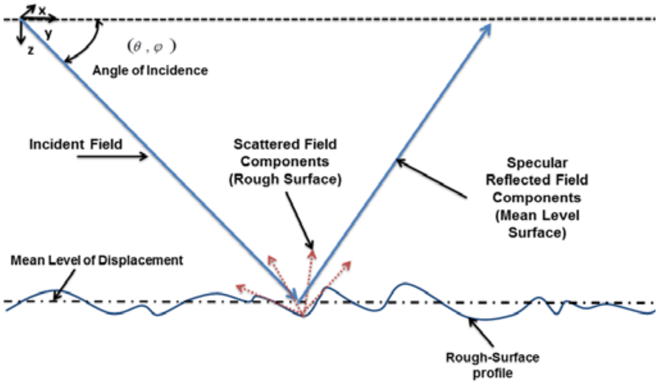
x
y
z
(θ , φ)
Angle of Incidence
Incident Field
Scattered Field Components (Rough Surface)
Specular Reflected Field Components (Mean Level Surface)
Mean Level of Displacement
Rough-Surface profile

Fig. B1. Description of rough-surface scattering phenomena

The electric field in the region defined by $z \le H - \varsigma(x,y)$ (Medium 1), illustrated in Fig. B1, can be written as

$$\mathbf{E}^{(1)}(\mathbf{r}) = \mathbf{E}_i e^{-j\mathbf{k}_{ti}\cdot\boldsymbol{\rho} - jk_{zi}z} + \mathbf{E}_{refl} e^{-j\mathbf{k}_{ti}\cdot\boldsymbol{\rho} + jk_{zi}(z-2H)} + e^{-jk_{zi}H} \iint d^2\mathbf{k}_t \mathbb{E}_s(\mathbf{k}_t, \mathbf{k}_{ti}) e^{-j\mathbf{k}_t\cdot\boldsymbol{\rho} + jk_z(z-H)}. \tag{B1}$$

The incident and reflected plane waves, $\mathbf{E}_i e^{-j\mathbf{k}_{ti}\cdot\boldsymbol{\rho} - jk_{zi}z}$ and $\mathbf{E}_{refl} e^{-j\mathbf{k}_{ti}\cdot\boldsymbol{\rho} + jk_{zi}(z-2H)}$, respectively, are characterized at the hypothetical plane $z = H$, and

$$\mathbf{E}^{(1)}_{scat}(\mathbf{k}_i, \mathbf{r}) = e^{-jk_{zi}H} \iint d^2\mathbf{k}_t \mathbb{E}_s(\mathbf{k}_t, \mathbf{k}_{ti}) e^{-j\mathbf{k}_t\cdot\boldsymbol{\rho} + jk_z(z-H)} \tag{B2}$$

is the rough-surface scattered field, which is also evaluated at the plane $z = H$. Similarly, the field quantities in Medium 2 are

$$\mathbf{E}^{(2)}(\mathbf{r}) = \mathbf{E}_{refr} e^{-jk_{zi}H} e^{-j\mathbf{k}_{ti}\cdot\boldsymbol{\rho} - jk_{2zi}(z-H)} + e^{-jk_{zi}H} \iint d^2\mathbf{k}_t \mathbb{E}^{(2)}_s(\mathbf{k}_t, \mathbf{k}_{ti}) e^{-j\mathbf{k}_t\cdot\boldsymbol{\rho} - jk_{2z}(z-H)}. \tag{B3}$$

Here, $\mathbf{E}_{refr} e^{-jk_{zi}H} e^{-j\mathbf{k}_{ti}\cdot\boldsymbol{\rho} - jk_{2zi}(z-H)}$ is a refracted plane wave traveling in Medium 2 and the field scattered into Medium 2 is written as

$$\mathbf{E}^{(2)}_{scat}(\mathbf{k}_i, \mathbf{r}) = e^{-jk_{zi}H} \iint d^2\mathbf{k}_t \mathbb{E}^{(2)}_s(\mathbf{k}_t, \mathbf{k}_{ti}) e^{-j\mathbf{k}_t\cdot\boldsymbol{\rho} - jk_{2z}(z-H)}. \tag{B4}$$

Note that the phase term $e^{-jk_{zi}H}$ was included in the expressions for the specular fields at $z = H$ to establish the phase reference at that location. This permits the reflected and refracted plane wave components (as well as $\mathbb{E}_s(\mathbf{k}_t, \mathbf{k}_{ti})$ and $\mathbb{E}^{(2)}_s(\mathbf{k}_t, \mathbf{k}_{ti})$) to be proportionate to the incident field via the Fresnel Reflection Coefficients. The purpose of $e^{-jk_{zi}H}$ can be explained easily explained in the context of transmission-line theory, where the antenna (input) port is the reference terminal plane and the load plane located at $z = H$. Here, the reflection (transmission) coefficient at load plane is referenced to the input reflection coefficient as represented in the specular terms of (B1) and (B3). We have also assumed that the rough surface scattered fields, as expressed using the Fourier expansion theorem, are valid within the region (i.e., the Rayleigh Hypothesis)

$$H - \min\varsigma(x,y) \le z \le H - \max\varsigma(x,y).$$

The boundary condition for the specularly reflected tangential electric-field components at H (i.e., $\varsigma(x,y) = 0$) is given as

$$\left(\mathbf{E}_i + \mathbf{E}_{refl} - \mathbf{E}_{refr}\right) \times \mathbf{z}_0 = 0. \tag{B5}$$

The corresponding magnetic-field expressions for both media have the given form of

$$\mathbf{H}^{(1)}(\mathbf{r}) = \mathbf{H}_i e^{-j\mathbf{k}_{ti}\cdot\boldsymbol{\rho} - jk_{zi}z} + \mathbf{H}_{refl} e^{-j\mathbf{k}_{ti}\cdot\boldsymbol{\rho} + jk_{zi}(z-2H)} + e^{-jk_{zi}H} \iint d^2\mathbf{k}_t \mathbb{H}_s(\mathbf{k}_t, \mathbf{k}_{ti}) e^{-j\mathbf{k}_t\cdot\boldsymbol{\rho} + jk_z(z-H)} \tag{B6}$$

for Medium 1, and

$$\mathbf{H}^{(2)}(\mathbf{r}) = \mathbf{H}_{refr} e^{-jk_{zi}H} e^{-j\mathbf{k}_{ti}\cdot\boldsymbol{\rho} - jk_{2zi}(z-2H)} + e^{-jk_{zi}H} \iint d^2\mathbf{k}_t \mathbb{H}^{(2)}_s(\mathbf{k}_t, \mathbf{k}_{ti}) e^{-j\mathbf{k}_t\cdot\boldsymbol{\rho} - jk_{2z}(z-H)} \tag{B7}$$

for Medium 2. In the above equations, the plane-wave spectral representations for the scattered magnetic fields are written as

$$\mathbf{H}^{(1)}_{scat}(\mathbf{k}_i, \mathbf{r}) = e^{-jk_{zi}H} \iint d^2\mathbf{k}_t \mathbb{H}_s(\mathbf{k}_t, \mathbf{k}_{ti}) e^{-j\mathbf{k}_t\cdot\boldsymbol{\rho} + jk_z(z-H)} \tag{B8}$$

and

$$\mathbf{H}^{(2)}_{scat}(\mathbf{k}_i, \mathbf{r}) = e^{-jk_{zi}H} \iint d^2\mathbf{k}_t \mathbb{H}^{(2)}_s(\mathbf{k}_t, \mathbf{k}_{ti}) e^{-j\mathbf{k}_t\cdot\boldsymbol{\rho} - jk_{2z}(z-H)}. \tag{B9}$$

Similarly, the boundary condition for the tangential components for the magnetic plane wave fields at the mean level $z = H$ is also given as

$$\left(\mathbf{H}_i + \mathbf{H}_{refl} - \mathbf{H}_{refr}\right) \times \mathbf{z}_0 = 0. \tag{B10}$$

In examining the phase term in (B2), (B4), (B8), and (B9), $e^{-jk_{zi}H}$ is treated as an arbitrary constant submitted in the expressions to give rise to a certain symmetry. It can also be said that each member of the spectral ensemble for the scattered fields is phase referenced to the plane $z = H$. Again, this step yields a symmetric set of solutions for the scattering amplitudes $\mathbb{E}^{(1,2)}_s(\mathbf{k}_t, \mathbf{k}_{ti})$ and $\mathbb{H}^{(1,2)}_s(\mathbf{k}_t, \mathbf{k}_{ti})$, which vanish when $\varsigma(x,y) = 0$. Note that the scale of $|\varsigma(x,y)|$ has yet to be specified; only the Rayleigh Hypothesis was enforced. The scattering amplitudes have a set of impedance relationships, which were derived from Maxwell's Equations and are given as

$$(\mathbf{k}_t - k_z\mathbf{z}_0) \times \mathbb{E}_s(\mathbf{k}_t, \mathbf{k}_{ti}) = \omega\mu_o \mathbb{H}_s(\mathbf{k}_t, \mathbf{k}_{ti}) \tag{B11}$$

and

$$\left(\mathbf{k}_t + k_{2z}\mathbf{z}_0\right)\times\mathbb{E}_s^{(2)}\left(\mathbf{k}_t,\mathbf{k}_{ti}\right) = \omega\mu_o\mathbb{H}_s^{(2)}\left(\mathbf{k}_t,\mathbf{k}_{ti}\right). \tag{B12}$$

Having defined the necessary parameters and field quantities in each medium, the solutions to the scattering amplitude for $\mathbb{E}_s\left(\mathbf{k}_t,\mathbf{k}_{ti}\right)$, and hence $\mathbb{H}_s\left(\mathbf{k}_t,\mathbf{k}_{ti}\right)$ can be determined by using (B1), (B3), (B6), and (B7) at $z = H - \varsigma\left(x,y\right)$ with the boundary conditions for the tangential field components, which are given by (B5), (B10), (B11), and (B12). These steps are shown as follows. The tangential electric-field components must be continuous at $z = H - \varsigma\left(x,y\right)$. Therefore, the boundary condition imposed on the surface is represented by the following expression,

$$\begin{gathered}\left[\left(\mathbf{E}_i\times\boldsymbol{\nu}_0\right)e^{jk_{zi}\varsigma(x,y)} + \left(\mathbf{E}_{refl}\times\boldsymbol{\nu}_0\right)e^{-jk_{zi}\varsigma(x,y)}\right]e^{-j\mathbf{k}_{ti}\cdot\boldsymbol{\rho}}\\ +\iint d^2\mathbf{k}_t\mathbb{E}_s\left(\mathbf{k}_t,\mathbf{k}_{ti}\right)\times\boldsymbol{\nu}_0 e^{-j\mathbf{k}_t\cdot\boldsymbol{\rho}-jk_z\varsigma(x,y)}\\ = \left(\mathbf{E}_{refr}\times\boldsymbol{\nu}_0\right)e^{-j\mathbf{k}_{ti}\cdot\boldsymbol{\rho}+jk_{2zi}\varsigma(x,y)} + \iint d^2\mathbf{k}_t\mathbb{E}_s^{(2)}\left(\mathbf{k}_t,\mathbf{k}_{ti}\right)\times\boldsymbol{\nu}_0 e^{-j\mathbf{k}_t\cdot\boldsymbol{\rho}+jk_{2z}\varsigma(x,y)},\end{gathered} \tag{B13}$$

for the electric field and

$$\begin{gathered}\left[\left(\boldsymbol{\nu}_0\times\mathbf{H}_i\right)e^{jk_{zi}\varsigma(x,y)} + \left(\boldsymbol{\nu}_0\times\mathbf{H}_{refl}\right)e^{-jk_{zi}\varsigma(x,y)}\right]e^{-j\mathbf{k}_{ti}\cdot\boldsymbol{\rho}}\\ +\iint d^2\mathbf{k}_t\boldsymbol{\nu}_0\times\mathbb{H}_s\left(\mathbf{k}_t,\mathbf{k}_{ti}\right)e^{-j\mathbf{k}_t\cdot\boldsymbol{\rho}-jk_z\varsigma(x,y)}\\ = \left(\boldsymbol{\nu}_0\times\mathbf{H}_{refr}\right)e^{-j\mathbf{k}_{ti}\cdot\boldsymbol{\rho}+jk_{2zi}\varsigma(x,y)} + \iint d^2\mathbf{k}_t\boldsymbol{\nu}_0\times\mathbb{H}_s^{(2)}\left(\mathbf{k}_t,\mathbf{k}_{ti}\right)e^{-j\mathbf{k}_t\cdot\boldsymbol{\rho}-jk_{2z}\varsigma(x,y)}\end{gathered} \tag{B14}$$

for the magnetic field. The outward normal is defined as

$$\boldsymbol{\nu}_0 = -\frac{\mathbf{z}_0 + \nabla_t\varsigma}{\sqrt{1+\left(\nabla_t\varsigma\right)^2}}. \tag{B15}$$

Next, the cancellation of $\sqrt{1+\nabla_t\varsigma\cdot\nabla_t\varsigma}$ on both sides of (B13) and (B14) is performed and the normal $\boldsymbol{\nu}_0$ is now set to $-\tilde{\boldsymbol{\nu}}_0 = \mathbf{z}_0 + \nabla_t\varsigma$. For convenience, the integration variable was changed from $\mathbf{k}_t$ to $\mathbf{k}_t^{'}$. A further modification is required to exploit a particular feature of $\varsigma\left(x,y\right)$ in the expressions above, in that

$$\begin{aligned}&-\iint d^2\mathbf{k}_t^{'}\mathbb{E}_s\left(\mathbf{k}_t^{'},\mathbf{k}_{ti}\right)\times\tilde{\boldsymbol{\nu}}_0 e^{-j\mathbf{k}_t^{'}\cdot\boldsymbol{\rho}}\\ &= \iint d^2\mathbf{k}_t^{'}\nabla_t\varsigma\times\mathbb{E}_s\left(\mathbf{k}_t^{'},\mathbf{k}_{ti}\right)e^{-j\mathbf{k}_t^{'}\cdot\boldsymbol{\rho}} + \iint d^2\mathbf{k}_t^{'}\mathbf{z}_0\times\mathbb{E}_s\left(\mathbf{k}_t^{'},\mathbf{k}_{ti}\right)e^{-j\mathbf{k}_t^{'}\cdot\boldsymbol{\rho}}\end{aligned} \tag{B16}$$

and

$$\begin{aligned}&-\iint d^2\mathbf{k}_t^{'}\mathbb{E}_s^{(2)}\left(\mathbf{k}_t^{'},\mathbf{k}_{ti}\right)\times\tilde{\boldsymbol{\nu}}_0 e^{-j\mathbf{k}_t^{'}\cdot\boldsymbol{\rho}}\\ &= \iint d^2\mathbf{k}_t^{'}\nabla_t\varsigma\times\mathbb{E}_s^{(2)}\left(\mathbf{k}_t^{'},\mathbf{k}_{ti}\right)e^{-j\mathbf{k}_t^{'}\cdot\boldsymbol{\rho}} + \iint d^2\mathbf{k}_t^{'}\mathbf{z}_0\times\mathbb{E}_s^{(2)}\left(\mathbf{k}_t^{'},\mathbf{k}_{ti}\right)e^{-j\mathbf{k}_t^{'}\cdot\boldsymbol{\rho}}\end{aligned} \tag{B17}$$

are added and subtracted from both sides of (B13), respectively. Equation (B13) is then re-expressed as

$$\begin{gathered}\left[\left(\mathbf{E}_i\times\tilde{\boldsymbol{\nu}}_0\right)e^{jk_{zi}\varsigma(x,y)} + \left(\mathbf{E}_{refl}\times\tilde{\boldsymbol{\nu}}_0\right)e^{-jk_{zi}\varsigma(x,y)}\right]e^{-j\mathbf{k}_{ti}\cdot\boldsymbol{\rho}}\\ +\iint d^2\mathbf{k}_t^{'}\mathbb{E}_s\left(\mathbf{k}_t^{'},\mathbf{k}_{ti}\right)\times\tilde{\boldsymbol{\nu}}_0 e^{-j\mathbf{k}_t^{'}\cdot\boldsymbol{\rho}}\left(e^{-jk_z^{'}\varsigma(x,y)}-1\right)\\ -\iint d^2\mathbf{k}_t^{'}\nabla_t\varsigma\times\mathbb{E}_s\left(\mathbf{k}_t^{'},\mathbf{k}_{ti}\right)e^{-j\mathbf{k}_t^{'}\cdot\boldsymbol{\rho}}\\ -\iint d^2\mathbf{k}_t^{'}\mathbf{z}_0\times\mathbb{E}_s\left(\mathbf{k}_t^{'},\mathbf{k}_{ti}\right)e^{-j\mathbf{k}_t^{'}\cdot\boldsymbol{\rho}}\\ = \left(\mathbf{E}_{refr}\times\tilde{\boldsymbol{\nu}}_0\right)e^{-j\mathbf{k}_{ti}\cdot\boldsymbol{\rho}+jk_{2zi}\varsigma(x,y)}\\ +\iint d^2\mathbf{k}_t^{'}\mathbb{E}_s^{(2)}\left(\mathbf{k}_t^{'},\mathbf{k}_{ti}\right)\times\tilde{\boldsymbol{\nu}}_0 e^{-j\mathbf{k}_t^{'}\cdot\boldsymbol{\rho}}\left(e^{jk_{2z}^{'}\varsigma(x,y)}-1\right)\\ -\iint d^2\mathbf{k}_t^{'}\nabla_t\varsigma\times\mathbb{E}_s^{(2)}\left(\mathbf{k}_t^{'},\mathbf{k}_{ti}\right)e^{-j\mathbf{k}_t^{'}\cdot\boldsymbol{\rho}}\\ -\iint d^2\mathbf{k}_t^{'}\mathbf{z}_0\times\mathbb{E}_s^{(2)}\left(\mathbf{k}_t^{'},\mathbf{k}_{ti}\right)e^{-j\mathbf{k}_t^{'}\cdot\boldsymbol{\rho}}.\end{gathered} \tag{B18}$$

Correspondingly, the magnetic field has a similar form to the above

$$\begin{gathered}\left[\left(\tilde{\boldsymbol{\nu}}_0\times\mathbf{H}_i\right)e^{jk_{zi}\varsigma(x,y)} + \left(\tilde{\boldsymbol{\nu}}_0\times\mathbf{H}_{refl}\right)e^{-jk_{zi}\varsigma(x,y)}\right]e^{-j\mathbf{k}_{ti}\cdot\boldsymbol{\rho}}\\ +\frac{1}{k_0Z_0}\iint d^2\mathbf{k}_t^{'}\tilde{\boldsymbol{\nu}}_0\times\left[\mathbf{k}'\times\mathbb{E}_s\left(\mathbf{k}_t^{'},\mathbf{k}_{ti}\right)\right]e^{-j\mathbf{k}_t^{'}\cdot\boldsymbol{\rho}}\left(e^{-jk_z^{'}\varsigma(x,y)}-1\right)\\ -\frac{1}{k_0Z_0}\iint d^2\mathbf{k}_t^{'}\nabla_t\varsigma\times\left[\mathbf{k}'\times\mathbb{E}_s\left(\mathbf{k}_t^{'},\mathbf{k}_{ti}\right)\right]e^{-j\mathbf{k}_t^{'}\cdot\boldsymbol{\rho}}\\ -\frac{1}{k_0Z_0}\iint d^2\mathbf{k}_t^{'}\mathbf{z}_0\times\left[\mathbf{k}'\times\mathbb{E}_s\left(\mathbf{k}_t^{'},\mathbf{k}_{ti}\right)\right]e^{-j\mathbf{k}_t^{'}\cdot\boldsymbol{\rho}}\\ = \left(\tilde{\boldsymbol{\nu}}_0\times\mathbf{H}_{refr}\right)e^{-j\mathbf{k}_{ti}\cdot\boldsymbol{\rho}+jk_{2zi}\varsigma(x,y)}\\ +\frac{1}{k_0Z_0}\iint d^2\mathbf{k}_t^{'}\tilde{\boldsymbol{\nu}}_0\times\left[\mathbf{k}_2'\times\mathbb{E}_s^{(2)}\left(\mathbf{k}_t^{'},\mathbf{k}_{ti}\right)\right]e^{-j\mathbf{k}_t^{'}\cdot\boldsymbol{\rho}}\left(e^{jk_{2z}^{'}\varsigma(x,y)}-1\right)\\ -\frac{1}{k_0Z_0}\iint d^2\mathbf{k}_t^{'}\nabla_t\varsigma\times\left[\mathbf{k}_2'\times\mathbb{E}_s^{(2)}\left(\mathbf{k}_t^{'},\mathbf{k}_{ti}\right)\right]e^{-j\mathbf{k}_t^{'}\cdot\boldsymbol{\rho}}\\ -\frac{1}{k_0Z_0}\iint d^2\mathbf{k}_t^{'}\mathbf{z}_0\times\left[\mathbf{k}_2'\times\mathbb{E}_s^{(2)}\left(\mathbf{k}_t^{'},\mathbf{k}_{ti}\right)\right]e^{-j\mathbf{k}_t^{'}\cdot\boldsymbol{\rho}}.\end{gathered} \tag{B19}$$

where k_0 is the free space wave number and $Z_0 = \sqrt{\frac{\mu_0}{\varepsilon_0}}$. The vector wave numbers $\mathbf{k}^{'}$ and $\mathbf{k}_2^{'}$ are defined as

$$\begin{aligned}\mathbf{k}^{'} &= \mathbf{k}_t^{'} - k_z^{'}\mathbf{z}_0;\\ \mathbf{k}_2^{'} &= \mathbf{k}_t^{'} - k_{2z}^{'}\mathbf{z}_0.\end{aligned} \tag{B20}$$

The impedance relationships given in (B11) and (B12) were used to obtain (B19). Note that the terms containing the factors $e^{\pm jk_z^{'}\varsigma(x,y)}-1$ and $e^{jk_{2z}^{'}\varsigma(x,y)}-1$ can be shown to be negligibly small compared to $O\left(\left|\nabla_t\varsigma\left(x,y\right)\right|\right)$. We now multiply both sides of (B18) with $\frac{1}{(2\pi)^2}e^{j\mathbf{k}_t\cdot\boldsymbol{\rho}}$ and integrate over the entire xy plane. Since,

$$\int e^{j\left(\mathbf{k}_t-\mathbf{k}_t^{'}\right)\cdot\boldsymbol{\rho}}d^2\boldsymbol{\rho} = \left(2\pi\right)^2\delta\left(\mathbf{k}_t-\mathbf{k}_t^{'}\right) \tag{B21}$$

we obtain

$$\begin{aligned}
&\int d^2\boldsymbol{\rho} e^{j(\mathbf{k}_t-\mathbf{k}_{ti})\cdot\boldsymbol{\rho}}\begin{Bmatrix}\left(\mathbf{E}_i\times\tilde{\boldsymbol{\nu}}_0\right)e^{jk_{zi}\varsigma(x,y)}+\left(\mathbf{E}_{refl}\times\tilde{\boldsymbol{\nu}}_0\right)e^{-jk_{zi}\varsigma(x,y)}\\ -\left(\mathbf{E}_{refr}\times\tilde{\boldsymbol{\nu}}_0\right)e^{jk_{2zi}\varsigma(x,y)}\end{Bmatrix}\\
&+\iint d^2\mathbf{k}_t'\int d^2\boldsymbol{\rho} e^{j\left(\mathbf{k}_t-\mathbf{k}_t'\right)\cdot\boldsymbol{\rho}}\begin{Bmatrix}\mathbb{E}_s\left(\mathbf{k}_t',\mathbf{k}_{ti}\right)\times\tilde{\boldsymbol{\nu}}_0\left(e^{-jk_z'\varsigma(x,y)}-1\right)\\ +\nabla_t\varsigma\times\mathbb{E}_s\left(\mathbf{k}_t',\mathbf{k}_{ti}\right)\end{Bmatrix}\\
&-\iint d^2\mathbf{k}_t'\int d^2\boldsymbol{\rho} e^{j\left(\mathbf{k}_t-\mathbf{k}_t'\right)\cdot\boldsymbol{\rho}}\begin{Bmatrix}\mathbb{E}_s^{(2)}\left(\mathbf{k}_t',\mathbf{k}_{ti}\right)\times\tilde{\boldsymbol{\nu}}_0\left(e^{jk_{2z}'\varsigma(x,y)}-1\right)\\ +\nabla_t\varsigma\times\mathbb{E}_s^{(2)}\left(\mathbf{k}_t',\mathbf{k}_{ti}\right)\end{Bmatrix}\\
&=(2\pi)^2\left\{\mathbf{z}_0\times\mathbb{E}_s^{(2)}\left(\mathbf{k}_t,\mathbf{k}_{ti}\right)-\mathbf{z}_0\times\mathbb{E}_s\left(\mathbf{k}_t,\mathbf{k}_{ti}\right)\right\}
\end{aligned}\tag{B22}$$

for (B18). A similar step performed on (B19) yields

$$\begin{aligned}
&k_oZ_0\int d^2\boldsymbol{\rho} e^{j(\mathbf{k}_t-\mathbf{k}_{ti})\cdot\boldsymbol{\rho}}\begin{Bmatrix}\left(\tilde{\boldsymbol{\nu}}_0\times\mathbf{H}_i\right)e^{jk_{zi}\varsigma(x,y)}+\left(\tilde{\boldsymbol{\nu}}_0\times\mathbf{H}_{refl}\right)e^{-jk_{zi}\varsigma(x,y)}\\ -\left(\tilde{\boldsymbol{\nu}}_0\times\mathbf{H}_{refr}\right)e^{jk_{2zi}\varsigma(x,y)}\end{Bmatrix}\\
&+\iint d^2\mathbf{k}_t'\int d^2\boldsymbol{\rho} e^{j\left(\mathbf{k}_t-\mathbf{k}_t'\right)\cdot\boldsymbol{\rho}}\begin{Bmatrix}\tilde{\boldsymbol{\nu}}_0\times\left[\mathbf{k}'\times\mathbb{E}_s\left(\mathbf{k}_t',\mathbf{k}_{ti}\right)\right]\left(e^{-jk_z'\varsigma(x,y)}-1\right)\\ +\nabla_t\varsigma\times\left[\mathbf{k}'\times\mathbb{E}_s\left(\mathbf{k}_t',\mathbf{k}_{ti}\right)\right]\end{Bmatrix}\\
&-\iint d^2\mathbf{k}_t'\int d^2\boldsymbol{\rho} e^{j\left(\mathbf{k}_t-\mathbf{k}_t'\right)\cdot\boldsymbol{\rho}}\begin{Bmatrix}\tilde{\boldsymbol{\nu}}_0\times\left[\mathbf{k}_2'\times\mathbb{E}_s^{(2)}\left(\mathbf{k}_t',\mathbf{k}_{ti}\right)\right]\left(e^{jk_{2z}'\varsigma(x,y)}-1\right)\\ +\nabla_t\varsigma\times\left[\mathbf{k}_2'\times\mathbb{E}_s^{(2)}\left(\mathbf{k}_t',\mathbf{k}_{ti}\right)\right]\end{Bmatrix}\\
&=(2\pi)^2\left\{\mathbf{z}_0\times\left[\mathbf{k}\times\mathbb{E}_s\left(\mathbf{k}_t,\mathbf{k}_{ti}\right)\right]-\mathbf{z}_0\times\left[\mathbf{k}_2\times\mathbb{E}_s^{(2)}\left(\mathbf{k}_t,\mathbf{k}_{ti}\right)\right]\right\}.
\end{aligned}\tag{B23}$$

With these given expressions, the final solution for the vector scattering amplitudes can be obtained by using a series of tedious algebraic steps (which will not be shown here). The final result is a solution to the Fredholm Integral equation of the second kind

$$\begin{aligned}
\begin{bmatrix}\mathbb{E}_s\left(\mathbf{k}_t,\mathbf{k}_{ti}\right)\\ \mathbb{E}_s^{(2)}\left(\mathbf{k}_t,\mathbf{k}_{ti}\right)\end{bmatrix}&=\int d^2\mathbf{k}_t'\begin{bmatrix}\mathbf{K}_{11}\left(\mathbf{k}_t',\mathbf{k}_t\right)&\mathbf{K}_{12}\left(\mathbf{k}_t',\mathbf{k}_t\right)\\ \mathbf{K}_{21}\left(\mathbf{k}_t',\mathbf{k}_t\right)&\mathbf{K}_{22}\left(\mathbf{k}_t',\mathbf{k}_t\right)\end{bmatrix}\begin{bmatrix}\mathbb{E}_s\left(\mathbf{k}_t',\mathbf{k}_{ti}\right)\\ \mathbb{E}_s^{(2)}\left(\mathbf{k}_t',\mathbf{k}_{ti}\right)\end{bmatrix}\\
&+\begin{bmatrix}\mathbf{V}_1\left(\mathbf{k}_t,\mathbf{k}_{ti}\right)\\ \mathbf{V}_2\left(\mathbf{k}_t,\mathbf{k}_{ti}\right)\end{bmatrix},
\end{aligned}\tag{B24}$$

where the first-order solutions for the scattering amplitudes are

$$\begin{aligned}
\begin{bmatrix}\mathbf{V}_1\left(\mathbf{k}_t,\mathbf{k}_{ti}\right)\\ \mathbf{V}_2\left(\mathbf{k}_t,\mathbf{k}_{ti}\right)\end{bmatrix}&=\begin{bmatrix}\mathbb{E}_s\left(\mathbf{k}_t,\mathbf{k}_{ti}\right)\\ \mathbb{E}_s^{(2)}\left(\mathbf{k}_t,\mathbf{k}_{ti}\right)\end{bmatrix}\\
&=\begin{bmatrix}\mathbf{T}_E^{(1)}\cdot\mathbf{V}_E\left(\mathbf{k}_t,\mathbf{k}_{ti}\right)+\mathbf{T}_H^{(1)}\cdot\mathbf{V}_H\left(\mathbf{k}_t,\mathbf{k}_{ti}\right)\\ \mathbf{T}_E^{(2)}\cdot\mathbf{V}_E\left(\mathbf{k}_t,\mathbf{k}_{ti}\right)+\mathbf{T}_H^{(2)}\cdot\mathbf{V}_H\left(\mathbf{k}_t,\mathbf{k}_{ti}\right)\end{bmatrix},
\end{aligned}\tag{B25}$$

and driving functions $\mathbf{V}_{E,H}\left(\mathbf{k}_t,\mathbf{k}_{ti}\right)$ are defined as

$$\mathbf{V}_E\left(\mathbf{k}_t,\mathbf{k}_{ti}\right)=\frac{-1}{(2\pi)^2}\int d^2\boldsymbol{\rho} e^{j(\mathbf{k}_t-\mathbf{k}_{ti})\cdot\boldsymbol{\rho}}\begin{Bmatrix}\left(\mathbf{E}_i\times\tilde{\boldsymbol{\nu}}_0\right)e^{jk_{zi}\varsigma(x,y)}+\left(\mathbf{E}_{refl}\times\tilde{\boldsymbol{\nu}}_0\right)e^{-jk_{zi}\varsigma(x,y)}\\ -\left(\mathbf{E}_{refr}\times\tilde{\boldsymbol{\nu}}_0\right)e^{jk_{2zi}\varsigma(x,y)}\end{Bmatrix}\tag{B26}$$

and

$$\mathbf{V}_H\left(\mathbf{k}_t,\mathbf{k}_{ti}\right)=\frac{-k_0Z_0}{(2\pi)^2}\int d^2\boldsymbol{\rho} e^{j(\mathbf{k}_t-\mathbf{k}_{ti})\cdot\boldsymbol{\rho}}\begin{Bmatrix}\left(\tilde{\boldsymbol{\nu}}_0\times\mathbf{H}_i\right)e^{jk_{zi}\varsigma(x,y)}+\left(\tilde{\boldsymbol{\nu}}_0\times\mathbf{H}_{refl}\right)e^{-jk_{zi}\varsigma(x,y)}\\ -\left(\tilde{\boldsymbol{\nu}}_0\times\mathbf{H}_{refr}\right)e^{jk_{2zi}\varsigma(x,y)}\end{Bmatrix}.\tag{B27}$$

Recall that under the small-slope constraint, $\left|\nabla_t\varsigma(x,y)\right|<<1$, $\tilde{\boldsymbol{\nu}}_0\sim 1$; and as a result, (B26) and (B27) reduce to (A7) and (A8) (in Appendix A), respectively. In examining (B22) and (B23), one should be reminded that there is no constraint on the scale of $\left|k_0\varsigma(x,y)\right|$, and thus, the continuity of the tangential electromagnetic field components hold at $z=H-\varsigma(x,y)$ as long as the Rayleigh Hypothesis is valid. Another consideration is that $\varsigma(x,y)$ is completely independent of H, and thus the scattered field lacks any phase continuity related to the difference between $\varsigma(x,y)$ and H. Therefore, any level shift perturbation of $\varsigma(x,y)$ (say by some constant $\pm h_0$) would be completely absorbed into H, and the formulation given in Appendix A, and herein would still apply.

Jimmy O. Alatishe was born in Washington, DC, in 1975. He received his B.S., M.S., and Ph.D degress in Electrical Engineering in 1998, 2000, and 2012, respectively, from The George Washington University in Washington, DC. His primary interest are in the areas of rough surface scattering and microwave circuits. He has been employed as a research engineer by the Radar Division at The Naval Research Laboratory in Washington, DC, Since 2000. His current efforts include research on the development of Radar recevier and transmitter modules, and advanced signal processing techniques.

Wasyl Wasylkiwskyj (F'97) received his BEE degree from the City University of New York in 1957, and the MS and Ph.D. degrees in electrical engineering from the Polytechnic University in 1965 and 1968, respectively. In 1984, after a 15 year career in private industry, where his last position was vice president and general manager of Physical Dynamics, Inc. in La Jolla California, he joined the George Washington University, Washington, DC, as Professor of Engineering and Applied Science. His research experience in the academic environment as well as a consultant to industry covers a broad spectrum of applied electromagnetics. This includes microwave components and techniques, phased-Array Antennas, EM propagation and scattering, radar cross-section modeling as well as modeling geophysical and oceanographic electromagnetic phenomena. In 1997 he was elected Fellow of IEEE for *“original contributions to electromagnetics, propagation and scattering and to fundamental understanding of phased-Array Antennas”*. His relativelty recent research was in direction finding algorithms with particular emphasis on the effects of mutual coupling on algorithm performance. The focus of his current research interests is in antennas for geophysical applications and scattering from random surfaces.